Cronfa - Swansea University Open Access Repository

_____

This is an author produced version of a paper published in:
Quaternary Science Reviews

_____

Cronfa URL for this paper:

_____

Paper:

Lovell, H., Benn, D., Lukas, S., Ottesen, D., Luckman, A., Hardiman, M., Barr, I., Boston, C. & Sevestre, H. (2018). Multiple Late Holocene surges of a High-Arctic tidewater glacier system in Svalbard. *Quaternary Science Reviews, 201*, 162-185.
http://dx.doi.org/10.1016/j.quascirev.2018.10.024

Multiple Late Holocene surges of a High-Arctic tidewater glacier system in Svalbard

Harold Lovell,[a*] Douglas I. Benn,[b] Sven Lukas,[c] Dag Ottesen,[d] Adrian Luckman,[e] Mark Hardiman,[a] Iestyn D. Barr,[f] Clare M. Boston[a] and Heidi Sevestre[b]

[a]*Department of Geography, University of Portsmouth, Portsmouth, UK*

[b]*School of Geography and Geosciences, University of St Andrews, St Andrews, UK*

[c]*Department of Geology, Lund University, Lund, Sweden*

[d]*Geological Survey of Norway, Trondheim, Norway*

[e]*Department of Geography, Swansea University, Swansea, UK*

[f]*School of Science and the Environment, Manchester Metropolitan University, Manchester, UK*

[*]**Corresponding author.** *E-mail: harold.lovell@port.ac.uk*

Abstract:

Most large tidewater glaciers in Svalbard are known to have surged at least once in the last few hundred years. However, very little information exists on the frequency, timing or magnitude of surges prior to the Little Ice Age (LIA) maximum in ~1900. We investigate the sediment-landform assemblages produced by multiple advances of the Nathorstbreen glacier system (NGS) in order to reconstruct its Late Holocene surge history. The glacier has recently undergone one of the largest surges ever observed in Svalbard, advancing ~16 km from 2008

to 2016. We present flow velocities and ice-marginal observations (terminus change, proglacial geomorphological processes) from the later stages of this surge. A first detailed assessment of the development of a glaciotectonic mud apron within the fjord during a surge is provided. Geomorphological and sedimentological examination of the terrestrial moraine areas formed prior to the most recent surge reveals that at least two advances were responsible for their formation, based on the identification of a previously unrecognised ice-contact zone recorded by the distribution of sediment facies in coastal exposures. We distinguish between an outer, older advance to the distal part of the moraine system and an inner, younger advance to a position ~2 km upfjord. Radiocarbon dating of shells embedded in glaciotectonic composite ridges formed by the onshore bulldozing of marine mud during the outer (older) of the two advances shows that it occurred at some point during the interval 700-890 cal. yr BP (i.e. ~1160 AD), and not during the LIA as previously assumed. We instead attribute the inner (younger) advance to the LIA at ~1890. By combining these data with previous marine geological investigations in inner and outer Van Keulenfjorden, we demonstrate that NGS has advanced at least four times prior to the recent 2008-2016 surge: twice at ~2.7 kyr BP, at ~1160 AD, and in ~1890. This represents a unique record of the timing and magnitude of Late Holocene tidewater glacier surges in Svalbard.

Keywords: glacier surge; glacial geomorphology; glaciology; Little Ice Age; Holocene; Svalbard

1. Introduction

Marine-terminating or tidewater glaciers in the High-Arctic archipelago of Svalbard have undergone accelerated mass loss in recent decades (Nuth et al., 2007, 2010; Błaszczyk et al., 2009; Carr et al., 2017). Most of these glaciers are known to experience flow instabilities called

surges (Sevestre and Benn, 2015), whereby they periodically undergo rapid advances for short periods of between three to ten years, before returning to a multi-decadal quiescent phase characterised by frontal thinning and retreat (Murray et al., 2003; Sund et al., 2009; Sevestre et al., 2018). Tidewater glacier surges result in rapid ice mass loss to the ocean and have a significant impact on the climate, oceanography, sediment budget, and geomorphology of fjord systems (e.g. Elverhøi et al., 1983; Hald et al., 2001; Plassen et al., 2004; Forwick et al., 2010).

The current state of knowledge on surging in Svalbard is largely based on observations from satellite imagery since the 1970s. Glacier surges pre-dating this are usually identified from aerial photographs (1930s onwards) or historical observations/written accounts (since the Little Ice Age (LIA) maximum ~1900) of characteristic surge evidence, such as widespread surface crevassing and/or rapid terminus advances (e.g. Liestøl, 1969; Hagen et al., 1993; Bennett et al., 1999; Ottesen et al., 2008; Flink et al., 2015). Very little is known about surge behaviour prior to the LIA maximum. In terms of general glacier behaviour at this time, some land-terminating glaciers in Svalbard are known to have experienced multiple episodes of ice expansion during the Late Holocene (i.e. since ~4 kyr BP) in response to a decline in summer insolation (Miller et al., 2017). The timings of maximum advances of tidewater glaciers during the Late Holocene display a large amount of variability across Svalbard. In some areas, such as inner Isfjorden, the LIA is thought to represent the Holocene maximum position (e.g. Plassen et al., 2004; Ottesen and Dowdeswell, 2006; Mangerud and Landvik, 2007). Other fjords record much older, more extensive tidewater advances (Hald et al., 2004; Evans and Rea, 2005; Kempf et al., 2013; Flink et al., 2017; Larsen et al., 2018). Many of these tidewater glaciers are inferred or known to be of surge-type, raising the question as to whether previous advances (LIA maximum or earlier) were glaciodynamic surges or were in response to climate forcing (e.g. Farnsworth et al., 2017; Philipps et al., 2017; Streuff et al., 2017a).

The best way to determine possible surging that predates observational records is by investigating sediment-landform assemblages, as surge behaviour is known to produce a diagnostic suite of landforms (Evans and Rea, 1999; Ottesen et al., 2017). Numerous studies have investigated englacial, geomorphological and sedimentological evidence exposed at the receding margins of quiescent phase surge-type glaciers in Svalbard in order to better understand the processes that occur during surges (e.g. Boulton et al., 1996, 1999; Glasser et al., 1998a; Bennett et al., 1999; Christoffersen et al., 2005; Larsen et al., 2006; Ottesen et al., 2008, 2017; Kristensen et al., 2009a,b; Lovell et al., 2015; Sobota et al., 2016; Larsen et al., 2018; Lyså et al., 2018). For tidewater glacier surges, this evidence is typically recorded on the sea floor (e.g. Solheim and Pfirman, 1985; Plassen et al., 2004; Ottesen et al., 2008, 2017; Forwick et al., 2010; Flink et al., 2015, 2017; Streuff et al., 2015, 2017a; Burton et al., 2016; Farnsworth et al., 2017). Field observations of the active phase of glacier surges are rare (e.g. Glasser et al., 1998b; Murray et al., 1998; Kristensen and Benn, 2012), but are crucial for linking surge processes to the geomorphological evidence left behind. This ensures interpretations based on exposed basal ice, englacial debris-rich structures, and/or sediment-landform assemblages (whether in marine or terrestrial positions) are more robust.

In order to contribute towards closing aforementioned gaps, we aim to reconstruct the history of Late Holocene advances in Van Keulenfjorden recorded within marine and terrestrial sediment-landform assemblages. We do this by investigating:

(1) active geomorphological processes at the glacier margin during a recent surge;

(2) the geomorphology of the terrestrial moraine areas in the inner fjord; and

(3) sediment facies exposed within the terrestrial moraine areas.

We combine this information with radiocarbon dating and previous marine geological investigations in order to produce a revised chronology of glacier advances.

2. Nathorstbreen glacier system (NGS) surge history

The Nathorstbreen glacier system (NGS) consists of several major tributary glaciers and currently terminates as a ~5 km-wide tidewater front in Van Keulenfjorden, a ~30 km-long fjord in southern Spitsbergen (77°30.55'N, 15°57.67'E) (Fig. 1). Nathorstbreen is the central and longest flow-unit (~39 km in 2017) in the system and drains from the accumulation area of Ljosfonn at an elevation of up to 700 m a.s.l. Radio echo sounding data from the 1980s indicate that NGS was over 300 m thick along its centre-line and warm based, with a cold surface layer up to 200m thick. The cold layer intersected with the bed in the terminal zone at this time (Dowdeswell et al., 1984). The other major NGS flow-units confluent with Nathorstbreen are Polakkbreen and Zawadzkibreen to the west and Dobrowolskibreen to the east. The system recently experienced the largest surge in Svalbard since the 1930s surges of Bråsvellbreen and Negribreen (Liestøl, 1969; Hagen et al., 1993), advancing >15 km from 2008 onwards and expanding onto the two moraine areas Nordre and Søre Nathorstmorenen at the lateral fjord margins (Fig. 1). Prior to this, the combined front of NGS (including neighbouring Liestølbreen and Doktorbreen) is thought to have advanced to more-extensive downfjord positions than reached in 2016 on at least three separate occasions: once during the Little Ice Age (LIA) in ~1870-80 (Ottesen et al., 2008) and twice at ~2.7 kyr BP (Kempf et al., 2013).

2.1 Recent surge

The recent NGS surge is described in detail in Sund et al. (2014) up until summer 2013, with the key details briefly summarised here. The combined tidewater terminus began to advance from inner Van Keulenfjorden sometime after October 2008 (Sund et al., 2014) (Fig. 1), signalling the onset of the frontal advance phase of the surge (stage 3 in Sund et al., 2009). Prior to this, surface measurements in 2000-01 showed that the upper basins of the four main

123   flow-units active during the surge (Nathorstbreen, Dobrowolskibreen, Polakkbreen and

124   Zawadzkibreen) were recording velocities of up to 1 m d^{-1}, representing an acceleration of the

125   order of 100 times' quiescent phase velocities of 0.01-0.02 m d^{-1} measured in 1992 (Sund et

126   al., 2014). This indicates that the early stages of surge initiation (stage 1 in Sund et al., 2009)

127   had begun in all contributing flow-units up to eight years before the start of the tidewater frontal

128   advance. Between 2003 and 2008, Dobrowolskibreen, Polakkbreen and Zawadzkibreen were

129   all observed to thin in their upper basins and thicken at lower elevations, demonstrating that

130   the downglacier propagation of mass was underway (stage 2 in Sund et al., 2009). The onset

131   of stage 2 in Dobrowolskibreen coincided with the appearance of large transverse crevasses in

132   the upper basin, which by 2006 were present all the way to the terminus of the flow-unit. By

133   2007, dense crevasse fields were also observed in the upper and middle parts of Zawadzkibreen

134   and had expanded to its entire length by 2008 (Ottesen *et al.*, 2008; Sund et al., 2014). By

135   contrast, surface crevassing of both Nathorstbreen and Polakkbreen was still limited in 2008

136   and did not become widespread until after the combined tidewater front had begun to advance

137   (Sund et al., 2014).

138   The first indications of terminus advance and calving were observed at the front of

139   Dobrowolskibreen in late 2007, followed by the abrupt advance of the combined terminus

140   sometime after October 2008 when velocities increased simultaneously (and by a factor of

141   three compared to 2007 values) within the Nathorstbreen and Zawadzkibreen flow-units (Sund

142   et al., 2009, 2014; Sund and Eiken, 2010). By September 2009, the terminus had advanced ~8

143   km at the centre-line into the deepest part of the inner fjord (~70 m according to pre-surge

144   bathymetry), representing the largest advance in a single year during the surge (Figs 1 and 2a).

145   The highest recorded velocities throughout the duration of the surge were also during this

146   period, averaging 20 m d^{-1} from March-May 2009 and 25 m d^{-1} from May-September 2009 at

147   the front (Sund et al., 2014). All four contributing flow-units appeared to advance at a similar

148 rate at this time, resulting in the combined front maintaining its overall shape and width and

149 precluding the development of looped moraines. By 2010, the terminus began to spread

150 towards the bay in front of the former tributaries Doktorbreen and Liestølbreen (not active

151 during the surge), with velocities reducing to 12.9 m d^{-1} across the front in the second part of

152 2010 (Sund et al., 2014). The terminus continued advancing northwards and by August 2011

153 had advanced onto Nordre Nathorstmorenen, effectively closing off the bay at the front of

154 Doktorbreen and Liestølbreen. From August 2011 until August 2012, the front advanced a

155 further ~1.5 km along the central axis of Van Keulenfjorden, recording average velocities of

156 ~5 m d^{-1} in the period 2011-12 (Sund et al., 2014). By July 2012, when fieldwork for this study

157 was conducted, the front had advanced into a shallow (~20 m deep according to pre-surge

158 bathymetry; Ottesen et al., 2008) and narrow part of the fjord and as a result ceased calving

159 (Figs 1 and 2b). In 2011-12 there was a reduction in both the rate of terminus advance (to ~1

160 m d^{-1}) and surface velocities, with velocities in winter 2012 (~2 m d^{-1}) about one-third of those

161 in winter 2011 (~6 m d^{-1}; Sund et al., 2014). Between December 2012 and January 2013, frontal

162 velocities remained ~2 m d^{-1} (Schellenberger et al., 2016). The front was still advancing in

163 August 2013 at the end of the period covered by the Sund et al. (2014) observations, and

164 extended ~0.9 km further downfjord compared to the August 2012 position. Between 2008 and

165 2013, NGS advanced a total of ~15 km (Fig. 1), with an additional ~3 km in length estimated

166 to have been lost through calving in the period 2009-2012 (Sund et al., 2014).

167

168 *2.2 Little Ice Age maximum surge*

169 There is evidence that NGS surged during the Little Ice Age (LIA) based on historical maps

170 and observations (Dunér and Nordenskiöld, 1865; Hamberg, 1905; Gripp, 1929), and marine

171 geological investigations (Ottesen et al., 2008). Photogrammetric mapping in 1898 by

172 Hamberg (1905) shows a tidewater glacier front with a large calving bay terminating ~3 km

173   upfjord from the northern extents of Nordre and Søre Nathorstmorenen (Fig. 1). An earlier map

174   by Dunér and Nordenskiöld (1865) shows the combined glacier front in 1864 terminating at a

175   position a further ~9 km upfjord from the 1898 terminus. From this, Ottesen et al. (2008)

176   inferred that NGS advanced sometime after 1864, and by 1898 was in the early stages of retreat

177   from the maximum position reached during this advance. The maximum position reached prior

178   to 1898 was suggested to be immediately downfjord of the northern extents of Nordre and Søre

179   Nathorstmorenen (Liestøl, 1973, 1977; Ottesen et al., 2008) (Fig. 1). This implies that between

180   1864 and 1898 NGS advanced ~12 km, followed by a retreat of ~3 km (Ottesen et al., 2008).

181   Assuming an average retreat rate comparable to the ~160 m a^{-1} that Nathorstbreen underwent

182   in the subsequent quiescent phase between 1898 and 2008 (~18 km in 110 years), this suggests

183   that the maximum position was reached ~15-20 years prior to 1898, in the late 1870s or early

184   1880s (Liestøl, 1973, 1977; Ottesen et al., 2008).

185   Several pieces of evidence suggest that the LIA advance was a surge. Firstly, the glacier

186   advanced ~12 km within a period of ~20 years, which is comparable in size and timescale to

187   the recent surge and a number of other observed surges of Svalbard glaciers (Murray et al.,

188   2003). Secondly, Hamberg (1905) mapped looped moraines on the glacier surface in 1898,

189   which are diagnostic of surges (cf. Meier and Post, 1969). Thirdly, swath bathymetry data from

190   inner Van Keulenfjorden presented by Ottesen et al. (2008) revealed a submarine landform

191   assemblage that is consistent with surging. This included: (i) glacial lineations, formed beneath

192   fast-flowing ice (e.g. King et al., 2009); (ii) a large terminal moraine located just beyond the

193   northern extents of Nordre and Søre Nathorstmorenen (Fig. 1), interpreted to be glaciotectonic

194   in origin (Ottesen et al., 2008); (iii) geometrical ridges, interpreted as crevasse squeeze ridges

195   formed by the injection of seafloor sediments into basal crevasses (e.g. Lovell et al., 2015); and

196   (iv) annual retreat moraines, marking minor winter readvances during terminus retreat in the

197   quiescent phase (e.g. Flink et al., 2015). This landform assemblage, or slight variations of it, is

198 found at the marine margins of several other known surge-type glaciers in Svalbard and is

199 suggested to be diagnostic of tidewater glacier surging (Ottesen et al., 2008, 2017; Flink et al.,

200 2015).

201

202 *2.3 Late Holocene maximum surge-like advances*

203 The large terminal moraine and debris flow lobe mapped by Ottesen et al. (2008), and assumed

204 to be of LIA age, were investigated and reinterpreted by Kempf et al. (2013) based on a

205 combination of swath bathymetry data, high-resolution seismics, and sediment cores. The

206 seismic data showed that the debris lobe actually consisted of two stacked units, which could

207 be correlated to a sediment core (JM07-014) collected from just beyond their distal margins

208 (Fig. 1). The age-depth model developed from the core indicates that both debris flow lobes

209 were deposited during a period of rapid sediment accumulation between 2.61 and 2.79 cal. kyr

210 BP, thus suggesting that these, and the terminal moraine complex, are considerably older than

211 the previously-assumed LIA age (Kempf et al., 2013). The implication is that the LIA surge

212 did not reach the crest of the terminal moraine complex, which was formed by the two ~2.7

213 kyr BP advances, as it would presumably have reworked the ridge and disturbed the debris

214 flow lobes. This was not apparent from the seismic profiles or the core. Instead, Kempf et al.

215 (2013) suggested that the LIA surge must have terminated to the east of the large moraine.

216 Kempf et al. (2013) concluded that the two advances at ~2.7 kyr BP were surge-like, and

217 estimated a time interval between deposition of the two lobes of ~100-150 years based on the

218 thickness of the acoustically stratified sediments. This is comparable to the modern NGS surge

219 return period of ~130 years.

220

221 **3. Methods**

222 The glacier margin from 2008-2017 was mapped from ASTER, Landsat (ETM+ and OLI) and

223 Sentinel-2 satellite imagery (acquired from earthexplorer.usgs.gov), apart from the 2009

224 margin, which was taken from Sund et al. (2014). Flow velocities were derived by feature-

225 tracking on TerraSAR-X (2013-2015) and Sentinel-1 (2015-2017) satellite image pairs. The

226 geomorphology of Nordre and Søre Nathorstmorenen was mapped from uncorrected 1:15,000

227 scale digital aerial photographs (acquired by the Norwegian Polar Institute (NPI) in summer

228 2011) and during fieldwork in July 2012 by adhering to the general mapping principles outlined

229 in Chandler et al. (2018). Sediment sections were cleaned before being logged as scaled two-

230 dimensional or vertical logs. Sediment facies were identified based on physical characteristics

231 (e.g. grain size range, sedimentary structures) following Evans and Benn (2004). Samples of

232 50 sandstone clasts were collected for clast shape and roundness analysis following Benn and

233 Ballantyne (1994). Clast shape data were plotted as ternary diagrams using TriPlot (Graham

234 and Midgley, 2000), clast roundness data were plotted as frequency distributions, and C_{40}, RA

235 and RWR indices were calculated (see Lukas et al., 2013). Bulk sediment samples were oven

236 (diamict) or freeze (mud) dried and dry-sieved to separate the fraction finer than 2 ϕ (250 µm).

237 The finer fraction was treated with hydrogen peroxide and disaggregated with a dispersing

238 agent before being analysed using a Beckman-Coulter Laser Sizer. These were plotted as grain

239 size distributions using GRADISTAT (Blott and Pye, 2001). Paired and individual bivalve

240 shells were radiocarbon dated at the [14]CHRONO Centre for Climate, the Environment and

241 Chronology at Queen's University Belfast. The radiocarbon ages were calibrated using OxCal

242 4.3 (Bronk Ramsey and Lee, 2013; Bronk Ramsey, 2017) and the internationally accepted

243 Marine13 radiocarbon calibration curve (Reimer et al., 2013), using a marine reservoir

244 correction with a ΔR value of 70±30 years (Mangerud et al., 2006; Mangerud and Svendsen,

245 2018). All radiocarbon ages are reported in the text as calibrated years before present (cal. yr

246 BP or cal. kyr BP). Key ages younger than 1000 cal. yr BP are also presented as years AD for

247 comparison with reported historical and modern dates. Bayesian modelling within OxCal 4.3

248 was used to produce a robust age estimation for the likely timing of an identified glacial

249 advance by constructing a simple '*Phase*' model. This included using selected radiocarbon

250 ages of bivalve shells, which are assumed to be slightly older than (or maximum-limiting) the

251 advance, and using the '*Boundary End*' age function within the model.

252

4. The surging margin of the Nathorstbreen glacier system (NGS)

254 During the recent surge, NGS advanced onto the terrestrial lateral moraine areas (Figs 1 and

255 2), providing a rare opportunity to observe ice-marginal processes during a surge and

256 investigate the geomorphological impact on the fjord and surrounding terrestrial areas.

257

258 *4.1 Frontal change and flow velocities 2013-2017*

259 The glacier front continued to advance from July 2013 until at least March 2016, showing that

260 the surge was still ongoing, albeit at a much-reduced rate of terminus change than in preceding

261 years (Figs 1 and 3). We measured flow velocities close to the front, recording an overall

262 deceleration from 2 m d^{-1} in early 2013 to ~0.1 m d^{-1} in late 2017, punctuated by dramatic

263 acceleration peaks in the summer months that coincide with precipitation events (Fig. 4). The

264 front advanced ~500 m in the centre of the fjord between July 2013 and July 2014. Flow

265 velocities increased abruptly in summer 2013 from ~2 m d^{-1} in June to ~5 m d^{-1} in July,

266 decreasing to <0.5 m d^{-1} in winter 2013-14 (Fig. 4). Frontal velocity peaked again at 4 m d^{-1} in

267 July 2014, before dropping to <0.5 m d^{-1} from September 2014 through to April 2015. A data

268 gap has resulted in no identifiable velocity peak in summer 2015, but the terminus advanced

269 ~300 m from July 2014 to July 2015 (Figs 3 and 4). The front continued to advance a further

270 ~200 m from July 2015 until March 2016. Velocities reduced from ~1 m d^{-1} in August 2015 to

271 <0.5 m d^{-1} in winter 2015-16 (Fig. 4). A further abrupt velocity increase occurred in summer

272   2016 from ~0.5 m d^{-1} in May to almost ~2.5 m d^{-1} in July (Fig. 4). Velocities reduced to ~0.5

273   m d^{-1} in late 2016 and to ~0.1 m d^{-1} in early 2017. As of August 2017, most of the glacier front

274   had receded relative to its 2016 position (Fig. 3), but it still experienced an abrupt summer

275   speed-up in July 2017 to ~1 m d^{-1}. By August 2017, velocities had reduced to ~0.1 m d^{-1},

276   comparable to pre-advance values in 2007. Together with the frontal recession, this indicates

277   that the active surge phase terminated sometime during winter 2016-17 (Figs 3 and 4). The

278   total advance during the 2008-2016 surge was ~16 km, with ~1 km of the advance occurring

279   in the later stages of the surge from 2013-2016 (Fig. 1).

280

281   *4.2 Ice margin observations in July 2012*

282   When fieldwork was conducted in July 2012, the central and most-extensive part of the

283   advancing terminus had reached a position approximately level with the distinct curved, spit-

284   like arm of Nordre Nathorstmorenen (Fig. 1). Despite having advanced onto the moraine areas,

285   the ice itself could not be accessed in 2012 due to the complex, fragmented nature of the

286   margin, the extensive areas of mud, and the presence of large (up to 15 m wide) and turbulent

287   meltwater channels along the full lengths of both lateral terrestrial margins (Figs 5, 6a and 6b).

288   Chaotic crevassing was observed across the ~10 km of the margin that was explored, including

289   the ~5 km of the front terminating in the fjord. Based on satellite images and aerial photographs

290   throughout the duration of the surge and observations from a helicopter flight over the glacier

291   in March 2011, this extended along the entire length of the terrestrial margin. The chaotic

292   crevassing was evident as large (ranging from ~5-30 m high), heavily-fractured blocks with

293   multiple distinct, typically sharp, pinnacles (Figs 6a and 6c). The orientation of the blocks and

294   pinnacles varied, ranging from vertical and near-vertical, those tilted at up to ~45° (in all

295   directions), through to those that had clearly toppled over and/or broken off. The latter were

296   typically debris-covered and formed dense groups stranded within the areas of mud and shallow

297   fjord waters at the margin. Due to this, there was no clearly-defined ice cliff (as found at calving

298   margins). Instead, the margin was heavily fragmented and stepped in height in most places,

299   increasing from ~2-5 m amongst the jumble of toppled and broken-off debris-covered blocks

300   up to ~20-30 m-high clean-ice pinnacles, often over a distance of tens of metres. Refrozen

301   breccias of smaller ice fragments and blocks were commonly observed within crevasses and

302   between large blocks, and some vertical and near-vertical crevasses contained muddy debris

303   extending up to tens of metres above the fjord level (Fig. 6b). Areas of debris-rich ice were

304   observed all along SW margin (Fig. 6b). Where the front terminated directly on the moraine

305   area, the moraine surface mostly appeared undisturbed, aside from at least one location at the

306   SW margin where part of the moraine had been excavated in front of the margin.

307

308   *4.3 Mud apron*

309   *4.3.1 Description* - A large area of seafloor mud located above the waterline first appeared

310   within the fjord across most of the tidewater front in summer 2012 (Figs 3 and 6), hereafter

311   referred to using the non-genetic term mud apron (Kristensen et al., 2009a). By mid-July 2012,

312   the mud apron extended up to 500 m in length from the NE margin and had begun to encroach

313   onto the spit-like arm of Nordre Nathorstmorenen (Figs 6c and 6d). The mud apron covered ~2

314   km^2 across the entire front at this time, and also extended upglacier at the SW lateral margin,

315   forming a ~10-20 m-wide border adjacent to the channel (e.g. Fig. 6b). Beyond the mud apron

316   in the centre of the fjord, the water was extremely turbid and <1 m deep ~1 km downfjord from

317   the glacier front (position marked by X in Fig. 3). The pre-surge water depth in this part of the

318   fjord was ~20 m (Fig. 1). The shallow water depth was also apparent from the large number of

319   icebergs stranded in turbid water in front of the margin, in addition to those surrounded by the

320   mud apron itself. Stranded icebergs were found all across the central part of the front and

321   towards the area where the SW lateral channel emerged into the fjord (Fig. 6e). The glacier

322 was clearly no longer calving into deep water across the entire front in July 2012, and the only

323 floating ice found in inner Van Keulenfjorden were tiny berglets transported into the fjord

324 along the lateral channels. The mud apron persisted in the fjord at the advancing margin from

325 July 2012 to March 2016, by which time it almost entirely covered the spit-like arm of Nordre

326 Nathorstmorenen (Fig. 3). Throughout this period, the mud apron was present at both the SW

327 and NE margins, and continued to be most extensive at the latter, but was not visible above the

328 waterline in the central part of the front. By August 2017, the margin had started to recede,

329 exposing parts of the mud apron that had been beneath the glacier in previous years (Fig. 3).

330 The surface of the mud apron was examined where it encroached onto the spit-like arm of

331 Nordre Nathorstmorenen (Figs 6c, 6d and 6f). It was characterised by flat areas of highly

332 saturated, slurry-like mud with frequent surface pools (Figs 6d and 6f) and running water. Flow

333 structures and small (~1 m high and several metres long) transverse ridges were also visible.

334 The sediment sampled from the mud apron (see Fig. 5 for sample locations) was a clayey silt,

335 with peaks in the medium and coarse-grain silt ranges (Fig. 7) and very few larger clasts. A

336 small lobe of the mud apron located on the moraine surface in summer 2012 was observed to

337 have advanced by tens of centimetres from one day to the next relative to marker cairns,

338 confirming that it was actively flowing in front of the advancing ice margin.

339

340 *4.3.2 Interpretation: glaciotectonic remobilisation of fjord-floor sediments -* The position,

341 morphology, and sedimentary characteristics of the mud apron are consistent with a

342 continuously-failing mobile moraine formed through the bulldozing of fjord-floor sediments

343 in front of the advancing glacier (Fig. 8). The lack of clasts within the mud apron indicate it

344 has a marine rather than a subglacial origin (e.g. Boulton et al., 1996; Kristensen et al., 2009a;

345 King et al., 2016). The formation of the mud apron is best explained by the tectonic thickening

346 of fjord-floor sediments in response to glacial push. The observed low gradient of both the

347 subaerial and submarine parts of the mud apron are consistent with the oversteepening and

348 failure of fjord-floor sediments with low shear strength (Kristensen et al., 2009a). The

349 transverse ridges within the mud apron, which are typically aligned parallel to the ice margin,

350 are interpreted as minor compressional ridges formed as a result of glacial push (Boulton et al.,

351 1996; Kristensen et al., 2009a). The presence of flow structures on the mud apron surface and

352 the measured apron advance of tens of centimetres a day indicate that it was actively flowing,

353 supporting the interpretation of a continuously-elevating and -failing sediment mass.

354

5. Geomorphology of Nordre and Søre Nathorstmorenen

356 Nordre and Søre Nathorstmorenen extend for ~15 km along both sides of inner Van

357 Keulenfjorden and cover a total area of ~40 km^2 (Figs 1 and 5). The moraine areas consist of

358 hummocky terrain with multiple ponds and sediment flows, networks of geometrical ridges,

359 and multi-crested composite ridge systems.

360

361 *5.1 Hummocky terrain*

362 *5.1.1 Description* - The terrain across both Nordre and Søre Nathorstmorenen is characterised

363 by hummocks and ridges interspersed with ponds, depressions and sediment flows, with a

364 typical elevation range of ~5-10 m (Figs 9a, 9b and 10a). Most of the topography consists of

365 irregular hummocks and ridges, which in places are interspersed with organised networks of

366 sharp-crested geometrical ridges (see *Section 5.2*). The ponds are widely distributed across both

367 moraine areas. At Nordre Nathorstmorenen, the densest grouping and largest ponds are located

368 in a broad corridor towards the distal margins of the hummocky terrain, whereas closer to the

369 active margin they tend to be smaller and more widely spaced (Fig. 5). The densest groupings

370 of ponds at Søre Nathorstmorenen are located at Søre Leirodden and at the fjord edge between

371 the two large outwash corridors that dissect the moraine area (Fig. 5). Sediment flows (Fig. 5),

372   exposed ice cores (Fig. 10b) and tension cracks within ridges, hummocks and the general

373   moraine surface (Fig. 10c) are found across both moraine areas. The dominant sediment facies

374   within the hummocky terrain are two diamicts with a wide range in grain sizes from mud to

375   large boulders, described in *Section 6*.

376

377   *5.1.2 Interpretation: Ice-cored terrain formed by subaerial stagnation during quiescence* – The

378   hummocky terrain records subaerial stagnation and de-icing of the glacier in a terrestrial

379   position. The melting of ice cores and degradation of the terrain surface through thermo-

380   erosional processes (cf. Etzelmüller et al., 1996) is evident across Nordre and Søre

381   Nathorstmorenen in the form of tension cracks and numerous sediment flows, indicative of

382   internal instabilities and sediment remobilisation (Lawson, 1982; Lukas et al., 2005). Complete

383   or partial melting of buried ice has also resulted in the widespread kettle topography of ponds

384   and drained depressions (akin to thermo-karst; Healy, 1975).

385

386   *5.2 Geometrical ridge networks*

387   *5.2.1 Description* - Dense groups or networks of predominantly sharp-crested ridges within

388   Nordre and Søre Nathorstmorenen are mapped as geometrical ridges (Figs 5, 9c, 9d and 10d).

389   These ridges were previously identified and described by Gripp (1929) as '*Lehmmauern*'

390   ('loam walls'; van der Meer, 2004). Individual ridges are typically 2-8 m high, 1-3 m wide and

391   ~50-100 m long. Ridge orientations are predominantly offset by 45º from, or sub-parallel to,

392   the central axis of the fjord (Fig. 5). The ridges display a variety of morphologies, ranging from

393   rounded elongate hummocks to free-standing vertical pinnacles or towers (Figs 10d-f). Sharp-

394   crested ridges and pinnacles are primarily located close to the active margin, such as in the area

395   around the spit-like arm of Nordre Nathorstmorenen (Figs 9c and 9d). The ridges become more

396   rounded in a downfjord direction towards Nordre and Søre Leirodden and towards the lateral

397 margins of the moraine areas, as also noted by Gripp (1929). As a result, geometrical ridges

398 are harder to distinguish from the general hummocky terrain in these areas. The ridges are

399 predominantly composed of diamict, described in *Section 6*.

400

401 *5.2.2 Interpretation: crevasse-squeeze ridges* – The geometrical ridge networks are interpreted

402 as crevasse-squeeze ridges, commonly observed at the submarine and terrestrial margins of

403 surge-type glaciers (e.g. Sharp, 1985; Boulton et al., 1996; Evans and Rea, 1999; Ottesen and

404 Dowdeswell, 2006; Ottesen et al., 2008, 2017; Lovell et al., 2015; Farnsworth et al., 2016;

405 Ingólfsson et al. 2016). Crevasse-squeeze ridges are formed by the injection of deformable

406 basal debris into vertical and near-vertical crevasses, as observed at the active ice margin (Fig.

407 6b). The ridges are then exposed and preserved at the margin as the glacier stagnates during

408 quiescence. This mechanism is most consistent with the formation of the sharp-crested ridges

409 and free-standing pinnacles observed in the moraine areas, and agrees with the interpretation

410 of Gripp (1929) for the same features.

411

412 *5.3 Composite ridge systems*

413 *5.3.1 Description* - Extensive areas of undulating topography with multiple linear ridge crests

414 are found at the distal margins of Nordre Nathorstmorenen, forming a sharp boundary with the

415 hummocky ice-cored terrain. These areas are identified as composite ridge systems based on

416 the following key geomorphological characteristics (cf. Lovell and Boston, 2017): their

417 comparatively smooth surface texture compared with the hummocky ice-cored terrain, the

418 orientation of ridge crests (which can be both perpendicular to and parallel with the fjord axis,

419 depending on whether the ridges are in a frontal or lateral position), and the deep channels that

420 are cut into them (Figs 5, 9a, 9b, 10g and 10h). The Nordre Nathorstmorenen composite ridge

421 systems are divided into the Nordre Leirodden and North-East (NE) systems (Figs 5, 9a and

422   9b). The Nordre Leirodden composite ridge system, which was briefly described by Gripp

423   (1929; in van der Meer, 2004: pp. 54-57), covers an area of ~2 km^2 and extends upglacier for

424   ~6 km from Nordre Leirodden at the NW margin of the moraine area (Fig. 5). The surface of

425   this part of the composite ridge systems reaches heights of up to 10 m above fjord/outwash

426   plain level and is dissected by several deep inactive channels (Fig. 9a). Low-amplitude ridge

427   crests are aligned sub-perpendicularly to the fjord axis close to Nordre Leirodden, and sub-

428   parallel to the fjord axis in a lateral position (Fig. 5). These ridge crests are very subdued and

429   reach typical heights of <0.5 m, and as a result are often difficult to identify in the field (Fig.

430   10g) but stand out on aerial photographs. The surface of the Nordre Leirodden composite ridge

431   system is composed predominantly of sand and gravel, with shells and shell fragments visible

432   in places. The NE composite ridge system is separated from the Nordre Leirodden system by

433   a large, inactive outwash corridor that joins the lateral outwash at the distal margins of the

434   moraine system (Fig. 5). The NE ridge system is also characterised by an undulating smooth

435   topography, dissected by multiple outwash corridors and reaching a height of ~5-10 m (Figs.

436   9b and 10h). The NE system extends along the lateral margins for ~6 km and reaches a

437   maximum width of ~1.5 km, in total covering ~5 km^2. Ridge crests and linear depressions are

438   typically aligned sub-perpendicularly to the fjord axis (Figs 5 and 9b). The biggest distinction

439   between the NE and Nordre Leirodden composite ridge systems is that the surface of the NE

440   system is composed of mud, with little to no sand and gravel (and no larger clasts) (Fig. 10h).

441   The mud is shell-rich with abundant shell fragments and complete paired bivalve shells

442   embedded in the surface.

443

444   *5.3.2 Interpretation: glaciotectonic moraines formed in a proglacial position* − The Nordre

445   Nathorstmorenen composite ridge systems are interpreted as glaciotectonic proglacial

446   moraines formed by glacier advance into foreland sediments (cf. Croot, 1988; Boulton et al.,

447 1999; Benediktsson et al., 2010; Lovell and Boston, 2017). The majority of the ridge crests,

448 certainly within the Nordre Leirodden ridges, are oriented parallel to the inferred ice-contact

449 face (boundary with the hummocky ice-cored terrain). This is consistent with ridge crests

450 formed perpendicular to the inferred direction of ice push (e.g. Hart and Watts, 1997; Boulton

451 et al., 1999; Lovell and Boston, 2017) as the glacier spread laterally towards the margins. The

452 smooth surface texture of the Nordre Nathorstmorenen composite ridge systems reflects their

453 surface sediment composition of sorted sand and gravel (Nordre Leirodden ridges) and mud

454 (NE ridges). Information on the internal structure of the Nordre Leirodden ridge system can be

455 found in *Section 6.3*.

456

457 6. Sedimentology of Nordre and Søre Nathorstmorenen

458 The sedimentary composition of the moraine areas was investigated within a series of sections,

459 mostly located at the fjord edge (Fig. 5). Five main sediment facies and facies associations

460 (FA) were identified: (1) shell-rich diamict (diamict 1); (2) shell-poor diamict (diamict 2); (3)

461 deformed fines (mud), sand and gravel (FA1) (4) undeformed fines (mud) and sand (FA2); and

462 (5) massive sand with contorted lenses (FA3). Information on grain size distributions, clast

463 shape, and clast roundness can be found in Fig. 7. Calibrated radiocarbon ages of shells are

464 reported here in relation to the sediment facies they were sampled from, and are discussed

465 further in *Section 7.2.3*.

466

467 *6.1 Diamict 1*

468 *6.1.1 Description* - Diamict 1 is the lowermost of two diamicts identified (Figs 11a and 12).

469 Diamict 1 is shell-rich, silty to fine-sandy, well-consolidated, matrix-supported, and contains

470 occasional boulders reaching maximum a-axis lengths of 1 m. Clasts within diamict 1 are

471 predominantly sub-angular and sub-rounded (Fig. 7), with striae common. This diamict is

472   typically structureless, but does contain thin clay stringers towards the distal parts of the

473   moraine areas, in particular close to the sharp boundary with the composite ridge systems

474   (composed of fine material) in Nordre Nathorstmorenen (e.g. section NNM01; Fig. 12a).

475   Diamict 1 was found both within geometrical ridges and coastal sections cut into the

476   hummocky terrain, but is restricted to the distal parts (downfjord ~1.5-2 km) of both moraine

477   areas. Within Nordre Nathorstmorenen, diamict 1 was not identified upfjord from section

478   NNM04, and diamict 1 was the only diamict identified in the downfjord (distal) ~1.5 km of

479   Søre Nathorstmorenen. Shells in diamict 1 were sampled for dating from Søre

480   Nathorstmorenen: two single *Hiatella arctica* shells from a coastal section returned ages of

481   5720-5870 and 10380-10660 cal. yr BP, and one pair of bivalve shells embedded in the moraine

482   surface at Søre Leirodden (Fig. 11f) returned ages of 1200-1290 and 1170-1260 cal. yr BP

483   (Table 1).

484

485   *6.1.2 Interpretation: lower till* - Based on its fine-grained matrix, presence of multiple shells,

486   and predominantly sub-angular to sub-rounded and striated clasts, diamict 1 is interpreted as a

487   till derived from marine sediment (cf. Boulton et al., 1996; Ó Cofaigh and Evans, 2001). Clay

488   lenses within the diamict at section NNM01 (Fig. 12a) are interpreted as evidence of the

489   incorporation and attenuation of underlying material into the basal zone during glacier

490   overriding (e.g. Kristensen et al., 2009a). Diamict 1 is interpreted to have been transported

491   subglacially during an advance that reached Nordre and Søre Leirodden.

492

493   *6.2 Diamict 2*

494   *6.2.1 Description* - Diamict 2 is matrix-supported and overlies diamict 1 at section NNM04

495   (Figs 11a and 12c), forming a sharp, erosional contact. The two diamicts can be differentiated

496   because diamict 2 is typically friable, poorly-consolidated and shell-poor, containing fewer and

497 more fragmentary shells than diamict 1. Thin, sometimes contorted, layers of sand and

498 occasional clay stringers are also common (e.g. Figs 11b, 12c and 13a). The main difference in

499 grain size distribution of diamicts 1 and 2 is the larger peaks within the coarse silt/fine sand

500 ranges displayed by diamict 2. Clast shape samples taken from sections NNM04 and SNM02

501 and from within geometrical ridges show predominantly sub-angular to sub-rounded clasts

502 (Fig. 7). Diamict 2 is the only diamict observed close to the active margin and is not found in

503 the distal parts of the moraine areas (e.g. downfjord from NNM04 and SNM01). Within Søre

504 Nathorstmorenen, the lateral transition in surface sediment cover from diamict 2 to diamict 1

505 is indistinct and, unlike at Nordre Nathorstmorenen, the two diamicts were not observed

506 together in section. Close to the active margin, diamict 2 is massive and sand lenses/clay

507 stringers are rare, but these increase in frequency in a downfjord direction (e.g. Figs 11b, 12c

508 and 13a). A single *Hiatella arctica* shell sampled from diamict 2 at Søre Nathorstmorenen (Fig.

509 5) returned an age of 7730-7860 cal. yr BP (Table 1).

510

511 *6.2.2 Interpretation: upper till* - Diamict 2 is interpreted as a second till derived from marine

512 sediment, deposited by a separate, less-extensive and more-recent glacier advance than that

513 associated with the deposition of diamict 1. Two main factors indicate that the diamicts relate

514 to separate advances: (1) at section NNM04, diamict 2 directly overlies diamict 1 and there is

515 a sharp, erosional contact between the two (Figs 11a and 12c). This indicates that the glacier

516 overrode and likely eroded diamict 1 following its deposition, emplacing diamict 2 on top. (2)

517 The spatial distribution of diamict 2 is restricted to the zones of sharp-crested geometrical

518 ridges close to the active margin, and it is not found in the distal parts of the moraine areas.

519 This is consistent with its deposition during a second, less-extensive glacier advance than that

520 which reached Nordre and Søre Leirodden and deposited diamict 1. The sand layers and clay

521 stringers within diamict 2 are interpreted as subglacially-reworked FA1 sediments (see *Section*

522 *6.3*).

523

524 *6.3 Deformed fines, sand and gravel facies (FA1)*

525 *6.3.1 Description* - This sediment facies association is exposed within the hummocky terrain

526 of both moraine areas (e.g. sections NNM01, NNM05, SNM01 and SNM02) and within the

527 Nordre Nathorstmorenen composite ridge systems (e.g. section NNM02) (Figs 12 and 13). It

528 is characterised by poorly-sorted sand with intercalated clay stringers, layers and lenses that

529 have been subject to minor faulting (e.g. NNM01; NNM05), shearing (e.g. SNM01) and/or

530 intense folding (e.g. NNM02; SNM02); faulted fine sand layers within a clay matrix (e.g.

531 NNM01); and clastic dykes and flame structures (e.g. NNM01 and NNM02). FA1 is found in

532 three main settings within the moraine areas, described below.

533   Firstly, FA1 underlies diamict 1 in both sections NNM01 and NNM05 within Nordre

534 Nathorstmorenen. The lowermost ~1.8 m of NNM01, located within the hummocky terrain

535 close to the boundary with the Nordre Leirodden composite ridge system, consists of FA1. This

536 includes a ~1.2 m section characterised by fine sand with thin clay stringers and shells

537 overlying shale bedrock. The shale is broken up and extremely friable, and angular clasts have

538 been ripped up from it and are present within the lowermost 0.2 m of the fine sand. Thin,

539 sinuous clastic dykes with flame-like structures are evident, trending upwards and towards the

540 true left of the section. A number of small-scale minor reverse faults can be identified,

541 particularly at a height of ~1 m, where the fine sand is laminated and contains small lenses of

542 black shale of a coarse sand grain size (Fig. 12a). The fine sand is overlain by ~0.6 m of massive

543 sand interspersed with discontinuous thin, faulted fine sand lenses.

544   Secondly, FA1 is also found close to the lateral transition between diamicts 1 and 2,

545 ~1.5-2 km upfjord from the distal margins of the moraine area. Coastal exposures in this part

546   of Søre Nathorstmorenen commonly contain deformed sands with sheared clay lenses (Fig.

547   11d) overlain by up to 1-2 m of diamict 2. At section SNM01 (Fig. 13a), ~1 m of diamict 2

548   containing several thin sand layers is overlain by ~0.5 m of FA1 in the form of sheared sand

549   with clay lenses. Approximately 200 m upfjord from this location, section SNM02 (Fig. 13b)

550   shows a ~1 m-wide layer of FA1, consisting of sands and thin clay lenses, forming a downfjord-

551   verging overturned fold around a core of diamict 2. The clay lenses within the sand and the

552   thin sand layers within diamict 2 are aligned parallel to the axial surface of the fold.

553   The third main location of FA1 is within the Nordre Nathorstmorenen composite ridge

554   systems. The internal composition of the Nordre Leirodden composite ridge system was

555   investigated in coastal exposures and logged in section NNM02 (Figs 11c and 12e). In coastal

556   exposures composed primarily of deformed sand, large-scale anticlinal folding was observed

557   in several places where bedding dipped in opposite directions over distances of tens of metres.

558   Sub-vertical muddy stringers and thrust and reverse faults with small displacements are also

559   common. At section NNM02, located in the wall of a channel cut through the Nordre Leirodden

560   ridges, FA1 is characterised by folded and contorted fine and coarse sand layers forming

561   attenuated synclines, with evidence for clastic dykes and flame structures (Fig. 12e).

562   Asymmetric folds are expressed on the surface of the Nordre Leirodden composite ridge system

563   as linear stripes or low-amplitude muddy ridge crests that stand-out against the general sandy-

564   gravelly surface (Fig. 10g). Several of these fold axes strike ~290º, comparable to fold axes

565   measured in section NNM02 (Fig. 12e). The internal structure of the NE composite ridge

566   system was not investigated, but the surface consisted of mud (massive clayey silt) (Fig. 7a).

567   Four paired shells of *Hiatella arctica* embedded in the NE composite ridge system surface (Fig.

568   11e) returned ages of 750-870, 830-950, 850-960 and 950-1110 cal. yr BP (Table 1).

569

570 *6.3.2 Interpretation: glaciotectonised shallow marine and fluvial sediments* - The massive and,

571 in places, laminated sands and shell-rich muds that contain evidence for faulting, folding and

572 shearing are interpreted as shallow marine, lacustrine and fluvial sediments that have been

573 glaciotectonically deformed in proglacial (e.g. NNM02 within the Nordre Leirodden composite

574 ridge system) and submarginal/subglacial (e.g. NNM01, NNM05, SNM01 and SNM02)

575 settings. FA1 sediments overlain by diamict 1 towards the distal margin of Nordre

576 Nathorstmorenen (NNM01 and NNM05) are interpreted as glaciotectonised shallow

577 marine/lacustrine sediments due to overriding and deformation as the glacier advanced to

578 Nordre and Søre Leirodden. The clastic dykes, flame structures (interpreted as water-escape

579 features) and reverse faulting within FA1 in section NNM01 are consistent with dewatering

580 and compaction caused by overlying ice (e.g. Phillips et al., 2008). FA1 sediments found in

581 conjunction with diamict 2 at the latter's downfjord limit in Søre Nathorstmorenen (e.g.

582 SNM01 and SNM 02) are similarly interpreted as evidence for the deformation of shallow

583 marine/lacustrine sediments in an ice-marginal position. The location of these sections, ~2 km

584 upfjord from the distal extent of the moraine system at Søre Leirodden indicates that they

585 represent a second former ice-contact zone. This is consistent with a second, less-extensive

586 glacier advance that deposited diamict 2. Deformed FA1 sediments are also found within the

587 glaciotectonic composite ridge systems of Nordre Nathorstmorenen. As the glacier advanced

588 downfjord and into terrestrial positions, it is likely to have encountered shallow marine

589 sediments within the fjord, lacustrine sediments in ponds on the moraine/glacier surface, and

590 outwash sediments. These sediments were then pushed and bulldozed into a series of ridges,

591 with ridge crests typically oriented perpendicular to the direction of ice push. The style of

592 folding and strike of fold axes within NNM02 (Fig. 12e) and exposed on the surface (Fig. 10g),

593 in conjunction with the general alignment of ridge crests on the Nordre Leirodden composite

24

594 ridge system (Figs 5 and 9a), are consistent with ice push from the south as the glacier advanced

595 into a terrestrial position and towards the lateral margins.

596

597 *6.4 Undeformed fines and sand (FA2)*

598 *6.4.1 Description* - FA2 is characterised by wavy laminated alternating couplets of clay-fine

599 silt grading into coarse silt-fine sand (NNM03; Figs 11g and 12b), ripple-bedded sands

600 (NNM03 and SNM03; Figs 12b and 13c), and massive clay, silt and sand (NNM03, NNM05

601 and SNM03). This facies association is found at the transition between the zones of diamicts 1

602 and 2 (i.e. where they are the predominant sediment facies) in both moraine complexes,

603 approximately 1.5 km upfjord from the distal margins. At section NNM03, located immediately

604 upfjord from the observed downfjord limit of diamict 2 within Nordre Nathorstmorenen, FA2

605 consists of a ~3 m-thick coarsening-upwards sequence of undisturbed wavy-laminated

606 alternating clay-fine silt couplets (~1 cm thick) (Fig. 11g), the uppermost ~1 m of which grades

607 into alternating silt-fine sand couplets (Fig. 12b). This sequence sits on top of bubbly, opaque

608 ice at least 0.2-0.3 m thick, and extends laterally for ~30 m. The laminated clays and silts are

609 overlain by a ~0.5 m-thick coarse sand layer with asymmetric ripples prograding in opposite

610 directions. Undeformed sorted sediments of FA2 are also found in section SNM03 in Søre

611 Nathorstmorenen, in a ~5-10 m-long exposure in a ridge located ~200 m from the fjord edge

612 (Fig. 5). Here, the lowermost 0.5 m of the exposure consists of wavy laminated alternating

613 couplets of fine and medium sand containing asymmetric ripples prograding in opposite

614 directions, interspersed with thin (<3 cm) horizontally-bedded lenses of fine gravel (Fig. 13c).

615

616 *6.4.2 Interpretation: undeformed shallow lacustrine sediments* - FA2 is consistent with

617 sediments of a shallow marine or shallow lacustrine origin. The wavy-laminated couplets

618 resemble tidally-influenced sediments (cf. Stewart, 1991), and the location of NNM03 at the

619   fjord edge suggests that the sediments may have been uplifted following deposition in the fjord.

620   However, the undeformed nature of the sediments and their height above the current fjord level

621   (up to ~3 m at NNM03) suggests that a marine origin is unlikely, as it is difficult to envisage a

622   mechanism by which uplift could have occurred with little or no disturbance of the sediments.

623   This is also the case for FA2 at SNM03, which is located ~300 m from the fjord and therefore

624   would have to have been transported a considerable distance without deformation. The absence

625   of shells within FA2 also suggests a marine origin is unlikely. Based on this, FA2 is most

626   consistent with undeformed shallow lacustrine sediments deposited *in situ* in ponds on the

627   former glacier or moraine surface that have since drained. NNM03 is underlain by glacier ice,

628   indicating deposition in a supraglacial pond before being lowered to the moraine surface. The

629   asymmetric ripples prograding in opposite directions within NNM03 and SNM03 are

630   consistent with delivery of underflows into a pond from changing sediment efflux points.

631

632   *6.5 Massive sand with contorted lenses (FA3)*

633   *6.5.1 Description* - FA3 is only observed at section SNM03, where it overlies, and has a sharp

634   contact with, the undeformed laminated sands of FA2. FA3 is characterised by a ~1.7 m-thick

635   layer of massive fine sand containing contorted coarse sand lenses and scattered gravel-sized

636   clasts (Fig. 13c). There is evidence for small rip-up clasts of medium sand within the lowermost

637   ~10-20 cm, sourced from the underlying laminated sands of FA2, and the thin lenses of coarser

638   sand within the otherwise fine sand matrix display a variety of shapes and alignments.

639

640   *6.5.2 Interpretation: subaerial sediment flow deposit* – FA3 is interpreted as a sediment flow

641   subjected to gravitational and water-sorting processes. This origin is consistent with the sharp,

642   erosional lower contact, homogenous nature of the fine sand matrix, the scattered gravel-sized

643   clasts, and the contorted coarse sand inclusions (cf. Lawson, 1982).

7. Discussion

7.1 Formation of mud apron and glaciotectonic surge moraines

The development of a mud apron during the recent surge of NGS provides a link between active phase processes and the formation of surge moraines, both in submarine and terrestrial positions. The emergence of the mud apron above the waterline in summer 2012 coincided with the glacier front reaching a narrow and shallow (~20 m) part of inner Van Keulenfjorden (Fig. 3), as noted by Sund et al. (2014). The extremely shallow water depths (<1 m) in the centre of the fjord in 2012 at ~1 km from the advancing margin demonstrate that a low gradient debris flow lobe extended downfjord from the subaerial part of the mud apron. Based on the pre-surge bathymetry (Fig. 1), the glacier front advanced up a reverse slope for ~10 km from the deepest part of inner Van Keulenfjorden in 2009 to its 2012 position. The soft marine sediments were pushed upslope as the front advanced, incrementally increasing the thickness of the sediment wedge over a distance of ~10 km through tectonic shortening (Fig. 8). By the time the glacier front reached the top of the reverse slope, i.e. at the shallowest part of the fjord, the sediment wedge was thick enough to breach the fjord surface. The advance against a reverse slope also explains why the mud apron is able to attain a significant thickness despite being composed of sediment with a very low shear strength and high porewater pressure, which might be expected to fail continuously (Kristensen et al., 2009a). The gravitational forces acting on the distal slope of the sediment wedge would be less influential than the lateral compression as it advanced upslope, therefore allowing the sediments to thicken. Once the glacier reached the top of the reverse slope and the bed began to slope away downfjord, gravitational processes exerted a larger influence on the sediment wedge and a low-gradient debris flow lobe developed through quasi-continuous slope failure (Kristensen et al., 2009a). It is interesting to note that Hamberg (1905) reported that in 1898 the water near Nordre Leirodden (Fig. 5)

669 contained stranded icebergs and was too shallow for boats due to the large amount of mud

670 deposited by the glacier. These observations are consistent with a mud apron within the fjord

671 associated with the 1898 position of NGS and reflect our own experience of navigating a boat

672 across the mud apron near the ice margin in 2012.

673   The mud apron that formed during the recent NGS surge is morphologically similar to

674 large submarine terminal moraines and associated debris flow lobes observed on the seafloor

675 in front of a number of tidewater surge-type glaciers (e.g. Solheim and Pfirman, 1985; Plassen

676 et al., 2004; Ottesen et al., 2008, 2017; Kristensen et al., 2009a; Forwick et al., 2010; Flink et

677 al., 2015; Streuff et al., 2015, 2017a; Burton et al., 2016), and we therefore interpret these as

678 having a common genetic origin (cf. Kristensen et al., 2009a). That is not to say that seafloor

679 sediments would have necessarily been pushed above the waterline during the formation of

680 surge terminal moraines in these other examples — this will depend on water depth. Aside

681 from Van Keulenfjorden, to our knowledge the only other report of mud pushed above the

682 waterline at an advancing glacier margin in Svalbard is from the 2002-10 surge of

683 Comfortlessbreen, which advanced ~700 m into the shallow water of Engelskbukta (King et

684 al., 2016; Lønne, 2016). However, such processes have been inferred during past surges of

685 Sefströmbreen (Boulton et al., 1996), Paulabreen (Kristensen et al., 2009a,b) and Osbornebreen

686 (Evans and Rea, 2005; Farnsworth et al., 2017) based on terrestrial geomorphological evidence.

687 Similar to these studies, the terrestrial composite ridge system at the lateral margin of Nordre

688 Nathorstmorenen is also inferred to have formed by a process of glaciotectonic pushing of

689 marine sediments onshore in front of an advancing ice margin. The grain size distribution of

690 the surface of the muddy part of the composite ridge system is very similar to that of the modern

691 mud apron (Fig. 7). Abundant shells on the surface of the ridges, many of which were paired

692 bivalve shells (Fig. 11e), also indicate a marine origin. The internal structure of this part of the

693 composite ridge system is unknown, but we note that the surface morphology is similar to the

694   terrestrial mud aprons/glaciotectonic moraines described by Boulton et al. (1996) and

695   Kristensen et al. (2009a,b).

696   There is a significant difference in the thickness of the active mud apron in terrestrial

697   areas, which was <10 cm thick where it had started to encroach onto Nordre Nathorstmorenen

698   (e.g. Fig. 6c), and the ~8-10 m high composite ridge system. Two main processes are likely to

699   explain this difference. Firstly, the sediments within the highly saturated, slurry-like active mud

700   apron have low shear strength, facilitating its continuous failure and the development of the

701   low-gradient debris flow lobe observed in both marine and terrestrial settings. By contrast,

702   large volumes of marine mud pushed further onshore would dewater, increasing the shear

703   strength of the mud. Subjected to continued push by an advancing ice margin, this would allow

704   the marine muds to be pushed into a series of steeper and higher ridges. Drying-out of marine

705   sediments can also result in extra cohesion caused by the crystallisation of salts (cf. Boulton et

706   al., 1996). Secondly, completely or partially frozen marine mud would have higher shear

707   strength than unfrozen mud, which could contribute to the coherence of the sediment mass

708   during proglacial deformation (e.g. Etzelmüller et al., 1996; Etzelmüller and Hagen, 2005).

709   The latter might be expected to form thrust-block moraines as the frozen sediments deformed

710   in a coherent manner, forming a series of thrust slabs (e.g. Evans and England, 1991).

711

712   *7.2 Late Holocene surge history of NGS*

713   Ottesen et al. (2008) used historical mapping and the submarine geomorphological record to

714   infer that NGS surged to a position downfjord of Nordre and Søre Nathorstmorenen in ~1870

715   (Ottesen et al., 2008; Fig. 1). This implies that the terrestrial moraine areas formed during the

716   LIA surge. The following sections demonstrate that Nordre and Søre Nathorstmorenen are

717   actually the result of two surges based on (1) the identification of two ice-contact zones

718   recorded by the distribution of sediment facies, facies associations and terrestrial

719 geomorphology; (2) the correlation between the ice-contact zones and submarine

720 geomorphology; and (3) radiocarbon dating of shells emplaced in a terrestrial position by the

721 outer, older surge.

722

723 *7.2.1 Identification of two ice-contact zones within the terrestrial moraine areas*

724 The sediment exposures record a downfjord transition from predominantly diamict 2 to a zone

725 of FA1 sediments, followed by a zone of predominantly diamict 1 extending to the distal part

726 of the moraine areas. In Nordre Nathorstmorenen only, the diamict 1 zone transitions into the

727 composite ridge systems comprising deformed FA1 sediments. In simple terms, we interpret

728 this as evidence of transitions (ice proximal to distal) from a subglacial zone (diamict 2) to a

729 submarginal/proglacial zone (FA1 in close association with diamict 2), back to a subglacial

730 zone (diamict 1), and finally to a proglacial glaciotectonised zone (FA1) within the composite

731 ridge systems. On this basis, two ice-contact zones can be identified at the subglacial-

732 submarginal/proglacial transitions (Fig. 14), which we attribute to two advances being

733 responsible for forming the terrestrial moraine areas. The second of these advances was less

734 extensive than the first, forming the inner ice-contact zone located ~2 km upfjord from the

735 distal extent of the moraine areas.

736   The transition from diamict 2 to FA1 deformed shallow marine sediments occurs at

737 approximately the same position within Nordre and Søre Nathorstmorenen (Fig. 14), which

738 delimits the former ice-contact zone (i.e. maximum downfjord position) of the inner advance.

739 This zone also coincides with the downfjord limit of the area of sharp-crested crevasse-squeeze

740 ridges (Figs 5 and 14) — beyond this, the ridges are, in general, more-rounded and typically

741 indistinguishable from the surrounding hummocky terrain of the moraine systems. We suggest

742 this reflects the differences in relative age of the crevasse-squeeze ridges formed by the inner,

743 younger advance and those formed during the outer, older advance to Nordre and Søre

744 Leirodden.

745   The ice-contact zone of the outer advance is located at the transition from hummocky

746 ice-cored terrain to composite ridge systems within Nordre Nathorstmorenen. This ice-contact

747 zone can be correlated with the downfjord extent of Søre Nathorstmorenen on the south side

748 of the fjord, delimiting the approximate maximum position of the outer advance (Fig. 14). The

749 lateral extents of the outer advance are constrained by the contact with the composite ridge

750 systems (Nordre Nathorstmorenen) and lateral limit of the moraine area (Søre

751 Nathorstmorenen). The lateral margins of the inner advance are harder to determine, as there

752 are no obvious geomorphological features (e.g. lateral meltwater channels or composite ridge

753 systems) that coincide with the ice-contact zones within either moraine system. It is possible

754 that the glacier extended to the lateral margins of both moraine areas. However, it seems likely

755 that the inner advance not only reached a less-extensive downfjord position, but also was

756 laterally less extensive. This is certainly the case for the recent surge, which reached a less-

757 extensive downfjord position and has only impinged on the lateral moraine areas by a few

758 hundred metres (Figs 1-3). In the absence of a clearly demarcated lateral margin for the inner

759 advance, we suggest it may coincide with observed differences in meltwater pond density. In

760 Nordre Nathorstmorenen, there is an identifiable corridor immediately adjacent to the fjord and

761 glacier margin that contains fewer meltwater ponds than the outermost part of the moraine

762 system (Fig. 5). This corridor widens from ~0.2 km at section NNM04 to ~1.5 km adjacent to

763 the 2012 glacier margin (Figs 5 and 14). We propose that the zone of fewer meltwater ponds

764 may represent the footprint of the inner advance. This is based on the logic that the relative

765 abundance of meltwater ponds in the outer, older parts of the moraine system reflect the longer

766 time it has had to de-ice and thus for ponds to develop. Søre Nathorstmorenen contains a similar

767 pattern, with dense areas of meltwater ponds located towards the distal margins, but the lateral

768   contrast is indistinct. We have therefore defined an approximate lateral extent of the inner

769   advance on Søre Nathorstmorenen based on a similar distance of encroachment onto the

770   moraine areas on both sides of the fjord (Fig. 14).

771

772   *7.2.2 Correlation of inner and outer advances with submarine geomorphology*

773   Based on the terrestrial evidence, it is logical to expect two separate advances to also be

774   recorded in the submarine geomorphology. The large submarine terminal ridge and associated

775   debris flow lobe mapped by Ottesen et al. (2008; Fig. 1), or at least the ice-proximal slope of

776   the ridge (cf. Kempf et al., 2013), correlates reasonably well with the maximum position of the

777   outer advance (i.e. the distal extent of the terrestrial moraine areas). However, Ottesen et al.

778   (2008) did not identify any terminal ridges or debris flow lobes in inner Van Keulenfjorden

779   that correlate to the inner advance. A series of small (average height of ~5 m) ridges aligned

780   broadly perpendicular to the fjord axis were identified and interpreted as annual moraines

781   formed during quiescent phase recession (Ottesen et al., 2008). Two of the largest of these

782   ridges are over 10 m high, ~500 m wide and are located either side of the position of the inner

783   ice-contact zone within the terrestrial moraine areas (labelled R1 and R2 in Fig. 14). The taller

784   of the two ridges (R1) corresponds closely to the position of the glacier front in 1898 mapped

785   by Hamberg (1905), which has the shape of a calving margin. We suggest this ridge is

786   consistent with a recessional moraine formed during quiescence (cf. Flink et al., 2015). Ridge

787   R2 is located ~1 km downfjord from the 1898 margin and immediately downfjord from the

788   approximate maximum position of the inner advance, as recorded within the terrestrial moraine

789   areas. Based on an assumed convex-shaped glacier front consistent with a surging margin (e.g.

790   Figs 1-3), we suggest that R2 is the most likely candidate to record the submarine position of

791   the inner advance maximum position (Fig. 14). Although R2 does not have a debris flow lobe

792   on its distal slope and is not as large as submarine terminal moraines identified at other

793   tidewater glaciers, we note that (i) debris flow lobes are not always found at surge terminal

794   moraines (e.g. Streuff et al., 2017a); and (ii) R2 is comparable in size and morphology to the

795   terminal moraine formed at the 2004 surge maximum position of Tunabreen in Tempelfjorden

796   (cf. Flink et al., 2015). In the latter case, Flink et al. (2015) concluded that where a surge follows

797   soon after a previous surge (e.g. ~40 years at Tunabreen), the glacier will not encounter as thick

798   glaciomarine sediment, and therefore will have less material available to bulldoze into a

799   terminal moraine. In addition, the velocity data from the final stages of the recent NGS surge

800   demonstrate that the glacier front experiences pulses of rapid flow acceleration in the summer

801   months during overall deceleration, probably during enhanced precipitation events as rainfall

802   is routed directly to the bed through the heavily-crevassed terminus (cf. Sevestre et al., 2018)

803   (Fig. 4). It is possible that most of the frontal advance in the later years occurs during these

804   concentrated periods of enhanced frontal velocities. Such a pulsing effect, possibly

805   characterised by parts of the front advancing whilst other areas are almost stationary (Fig. 3),

806   may well have an impact on the size and morphology of any submarine moraines formed at the

807   margin.

808

809   *7.2.3 Revised chronology of surging*

810   Glacier surges are separated by multi-decadal periods of quiescent phase recession. The two

811   advances recorded within the moraine areas are therefore expected to be of different ages. The

812   oldest radiocarbon ages of 10380-10660, 7730-7860 and 5720-5870 cal. yr BP (Table 1) were

813   from individual shells embedded in diamicts 1 and 2 in coastal sections within Søre

814   Nathorstmorenen. These are considerably older than the two advances dated to between 2610

815   and 2790 cal. yr BP that formed the large submarine terminal moraine and debris flow lobes in

816   outer Van Keulenfjorden (Kempf et al., 2013; Fig. 1), suggesting that the shells have undergone

817   significant (e.g. multiple cycles of) remobilisation and redeposition (Lyså et al., 2018). The

818   remaining ages were from four sets of paired bivalve shells sampled from the surface of the

819   NE composite ridge system (750-870, 830-950, 850-960 and 950-1110 cal. yr BP; Table 1) and

820   one set of paired bivalve shells embedded in the moraine surface at the distal extent of Søre

821   Nathorstmorenen (1200-1290 and 1170-1260 cal. yr BP; Table 1). The NE composite ridge

822   system is interpreted to have formed by onshore bulldozing of marine mud in a proglacial

823   position during the outer, assumed older, advance. Similarly, the paired bivalve shells

824   embedded in the surface of Søre Nathorstmorenen are within the part of the moraine complex

825   formed by the outer advance (Fig. 14). We use the four, slightly younger ages from the NE

826   composite ridge system to produce a robust modelled age for the outer advance occurring

827   during the period 700-890 cal. yr BP (Fig. 15), or sometime around ~1160 AD.

828   The inner advance corresponds closely to the 1898 glacier front (Fig. 14). Similar to

829   Ottesen et al. (2008), we interpret the 1898 position as representing the initial stages of frontal

830   recession following a late 19th century surge. However, we have identified that this surge did

831   not extend to the distal part of the moraine system as previously thought, but terminated ~2 km

832   upfjord at our proposed maximum position of the inner advance (Fig. 14). By 1898 the glacier

833   front in the centre of the fjord had calved back ~1-1.5 km from the likely surge maximum

834   position. If we assume a quiescent phase recession rate of ~160 m a^{-1} (as recorded in the period

835   1898 to 2008), the inner advance likely reached its maximum position ~6-10 years prior to

836   1898, suggesting the LIA surge occurred ~1890. We therefore determine that NGS has surged

837   at least five times: twice between 2.61 and 2.79 cal. kyr BP (Kempf et al., 2013), at ~1160 AD,

838   in ~1890, and from 2008-2016 AD (Fig 16).

839

840   *7.3 Timings of Late Holocene tidewater glacier advances in Svalbard*

841   There are very few records of the timings of Late Holocene tidewater glacier advances in

842   Svalbard before the LIA maximum. Indeed, prior to an inferred ~1800 AD surge of

843   Kongsvegen/Kronebreen in Kongsfjorden (Liestøl, 1988), only six glacier systems have had

844   dated advances since the onset of the neoglacial period at ~4 kyr BP (Hald et al., 2004) (Fig.

845   16). The oldest dated advances since ~4 kyr BP are the two advances of NGS between 2.61

846   and 2.79 cal. kyr BP, which were interpreted as surges (Kempf et al., 2013). The Hinlopen-

847   Oslobreen glacier systems in Vaigattbogen also surged sometime prior to 2.6 cal. kyr BP,

848   although this could have occurred at any point since the early Holocene (Flink and Noormets,

849   2018). In Hornsund, southern Spitsbergen, a tidewater glacier advance to the Treskelen

850   Peninsula was dated to 1.9±0.3 kyr BP using [10]Be cosmogenic nuclide dating (Philipps et al.,

851   2017). Philipps et al. (2017) suggested this advance was likely to be in response to regional

852   climate forcing rather than a surge, although they also noted that several of the glaciers feeding

853   into Hornsund are reported to have surged at or since the LIA. Also in southern Spitsbergen,

854   Paulabreen in Van Mijenfjorden surged ~650 yr BP (~1300 AD) (Hald et al., 2001; Larsen et

855   al., 2018). This surge formed the terrestrial glaciotectonic moraine systems of Damesmorenen,

856   Crednermorenen and Torelmorenen through onshore bulldozing of marine mud (Kristensen et

857   al., 2009a; Larsen et al., 2018; Lyså et al., 2018). Based on the submarine geomorphological

858   record (Ottesen et al., 2008), Paulabreen surged at least twice more between the dated ~1300

859   AD surge and an inferred surge in ~1898 (Larsen et al., 2018). In northwest Spitsbergen, St.

860   Jonsfjorden and Magdalenefjorden both have tidewater glacier advances dated to before the

861   LIA (Farnsworth et al., 2017; Streuff et al., 2017a). Osbornebreen in St. Jonsfjorden advanced

862   and deposited a moraine dated to ~520±70 cal. yr BP (~1430 AD), which has been interpreted

863   as a surge based on the terrestrial and submarine geomorphological record (Evans and Rea,

864   2005; Farnsworth et al., 2017). In Magdalenefjorden, Waggonwaybreen advanced at ~300 cal.

865   yr BP (~1650 AD) (Streuff et al., 2017a). The submarine geomorphology was interpreted by

866   Streuff et al. (2017a) to be more consistent with this advance being a response to LIA cooling

867   rather than a surge. Both Paulabreen and NGS are inferred to have surged at the end of the LIA

868   maximum (Ottesen et al., 2008) and have surged in the last 15 years (Kristensen and Benn,

869   2012; Sund et al., 2014). Osbornebreen also underwent an observed surge in 1986-1988

870   (Dowdeswell et al., 1991).

871   The recent expansion in the availability of high-resolution submarine imagery has

872   helped to identify new evidence for dynamic glacier flow in both fjord (Ottesen and

873   Dowdeswell, 2006; Ottesen et al., 2008; Flink et al., 2015, 2017; Streuff et al., 2015, 2017a;

874   Burton et al., 2016; Ewertowski et al., 2016; Farnsworth et al., 2017; Allaart et al., 2018;

875   Ćwiąkała et al., 2018; Larsen et al., 2018) and open-marine settings (Ottesen et al., 2017; Flink

876   and Noormets, 2018). In the majority of these examples, there is clear geomorphological

877   evidence for surging. As more areas are explored, it seems likely that such observations will

878   increase. However, chronological control on the timing of advances is crucial in order to

879   understand tidewater glacier behaviour during the Late Holocene. From the available data, it is

880   clear that there is a great deal of variability across Svalbard. In some areas (e.g. inner Isfjorden,

881   Lomfjorden), the LIA maximum is thought to represent the most-extensive Holocene glacier

882   position (Plassen et al., 2004; Ottesen and Dowdeswell, 2006; Mangerud and Landvik, 2007;

883   Streuff et al., 2017b). By contrast, glaciers in Mohnbukta experienced a surge-type advance

884   prior to 7.7 cal. kyr BP (Flink et al., 2017), and both NGS (Kempf et al., 2013 and this study)

885   and Paulabreen (Larsen et al., 2018; Lyså et al., 2018) surged at least three times prior to the

886   LIA to more advanced positions than their LIA maximums. In terrestrial settings, Farnsworth

887   et al. (2018) established that several land-terminating glaciers in Svalbard re-advanced during

888   the late-glacial to early-Holocene period, reaching positions up to ~8 km beyond their Late

889   Holocene maximum moraines, and Miller et al. (2017) identified several episodes of land-

890   terminating glacier expansion during the Late Holocene. Understanding these variations in the

891   timings of glacier maxima during the Holocene is important in order to understand glacier

892 behaviour over longer timescales, and in particular the interplay between climatic forcing and

893 glaciodynamical (i.e. surging) influences on glacier advances.

894

9. Conclusions

896 Investigation of terrestrial and submarine sediment-landform assemblages in Van

897 Keulenfjorden, southern Spitsbergen, reveal a Late Holocene record of multiple advances of

898 the surge-type Nathorstbreen glacier system (NGS).

899 • NGS advanced ~16 km from 2008 to 2016 during its recent surge. The final years of

900   the surge (2013-2016) were characterised by year-on-year decreases in flow velocities

901   punctuated by occasional, short-lived speed-ups (e.g. fivefold increases) correlated to

902   summer precipitation events. By August 2017, NGS had started to retreat across most

903   of the front, indicating surge termination sometime in winter 2016-2017.

904 • We present the first detailed observations of the formation of a glaciotectonic mud

905   apron in the fjord during the recent surge. The mud apron emerged above the waterline

906   and began to encroach onto the lateral moraine areas in summer 2012. The mud apron

907   was caused by the bulldozing and thickening of marine sediments into a mobile,

908   continuously failing sediment wedge characterised by a low-gradient flow lobe

909   extending downfjord. These observations provide a modern analogue for the formation

910   of submarine terminal surge moraines and associated debris flow lobes, and terrestrial

911   glaciotectonic moraine systems formed by the onshore movement of marine sediments

912   during glacier surges.

913 • Investigation of the sediment-landform assemblages within the terrestrial moraine areas

914   reveals that at least two separate phases of glacier advance are recorded. This is based

915   on the identification of an additional, previously unrecognised, ice-contact zone

916   characterised by a transition from subglacial sediments to proglacially/submarginally

deformed sediments. We infer that this records an inner, younger advance that did not extend to the distal parts of the moraine system.

- Radiocarbon dating of shells embedded in the surface of the glaciotectonic composite ridge systems at the distal margins of the terrestrial moraine area indicate that the outer, older advance occurred at ~1160 AD, rather than during the LIA as previously suggested by Ottesen et al. (2008). We instead correlate the inner, younger advance to the LIA and suggest it culminated in ~1890 based on the position of the calving (retreating) glacier terminus mapped by Hamberg (1905) in 1898.

- We demonstrate that NGS has advanced at least five times in the Late Holocene: (1) the recent surge advance of 2008-2016, (2) during the LIA at ~1890, (3) at ~1160 AD, and (4) and (5) twice between 2.61 and 2.79 cal. kyr BP, as previously reported by Kempf et al. (2013).

In addition to the recent 2008-2016 surge, the observed sediment-landform assemblages associated with the four older advances are also consistent with surging. This work contributes to the understanding of High-Arctic tidewater glacier dynamics, and in particular the frequency and magnitude of surge advances, during the Late Holocene. Future work should focus on combined marine and terrestrial investigations at the margins of other tidewater glaciers in order to provide a more complete picture of the regional variability in Holocene glacier advances in Svalbard.

CRediT author statement

HL, **DIB**, **SL**: Conceptualization, Methodology, Investigation, Writing – Original Draft. **DO**, **AL**: Investigation, Resources, Writing – Review & Editing. **MH**: Methodology, Formal Analysis, Writing – Review & Editing. **IDB**: Resources, Writing – Review & Editing. **CMB**, **HS**: Writing – Review & Editing.

References

Allaart, L., Friis, N., Ingólfsson, Ó., Håkansson, L., Noormets, R., Farnsworth, W.R., Mertes, J., Schomacker, A., 2018. Drumlins in the Nordenskiöldbreen forefield, Svalbard. GFF 1-19.

Benediktsson, Í.Ö., Schomacker, A., Lokrantz, H., Ingólfsson, Ó., 2010. The 1890 surge end moraine at Eyjabakkajökull, Iceland: a re-assessment of a classic glaciotectonic locality. Quaternary Science Reviews 29, 484-506.

Benn, D.I., Ballantyne, C.K., 1994. Reconstructing the transport history of glacigenic sediments: a new approach based on the co-variance of clast form indices. Sedimentary Geology 91, 215-227.

966   Bennett, M.R., Hambrey, M.J., Huddart, D., Glasser, N.F., Crawford, K., 1999. The landform

967   and sediment assemblage produced by a tidewater glacier surge in Kongsfjorden,

968   Svalbard. Quaternary Science Reviews 18, 1213-1246.

969   Błaszczyk, M., Jania, J.A., Hagen, J.O., 2009. Tidewater glaciers of Svalbard: Recent changes

970   and estimates of calving fluxes. Polish Polar Research. 30, 85-142.

971   Blott, S.J., Pye, K., 2001. GRADISTAT: a grain size distribution and statistics package for the

972   analysis of unconsolidated sediments. Earth Surface Processes and Landforms 26, 1237-

973   1248.

974   Boulton, G.S., van der Meer, J.J.M., Hart, J.K., Beets, D.J., Ruegg, G.H.J., van der Wateren,

975   F.M., Jarvis, J., 1996. Till and moraine emplacement in a deforming bed surge - an

976   example from a marine environment, Quaternary Science Reviews 15, 961-987.

977   Boulton, G.S., van der Meer, J.J.M., Beets, D.J., Hart, J.K., Ruegg, G.H.J., 1999. The

978   sedimentary and structural evolution of a recent push moraine complex:

979   Holmstrømbreen, Spitsbergen, Quaternary Science Reviews 18, 339-371.

980   Bronk Ramsey, C., 2017. OxCal Program, Version 4.3. Available at https://c14.arch.ox.ac.uk/.

981   Bronk Ramsey, C., Lee, S., 2013. Recent and planned developments of the program OxCal.

982   Radiocarbon 55, 720–730.

983   Burton, D.J., Dowdeswell, J.A., Hogan, K.A., Noormets, R., 2016. Marginal fluctuations of a

984   Svalbard surge-type tidewater glacier, Blomstrandbreen, since the Little Ice Age: a record

985   of three surges. Arctic, Antarctic, and Alpine Research 48, 411-426.

986   Carr, J.R., Stokes, C.R., Vieli, A., 2017. Threefold increase in marine-terminating outlet glacier

987   retreat rates across the Atlantic Arctic: 1992–2010. Annals of Glaciology 58, 72-91.

988   Chandler, B.M.P., Lovell, H., Boston, C.M., Lukas, S., Barr, I.D., Benediktsson, Í.Ö., Benn,

989   D.I., Clark, C D., Darvill, C.M., Evans, D.J.A., Ewertowski, M.W., Loibl, D., Margold,

990   M., Otto, J-C., Roberts, D.H., Stokes, C.R., Storrar, R.D., Stroeven, A.P., 2018. Glacial

991   geomorphological mapping: a review of approaches and frameworks for best practice.

992   Earth-Science Reviews

993   Christoffersen, P., Piotrowski, J.A., Larsen, N.K., 2005. Basal processes beneath an Arctic

994   glacier and their geomorphic imprint after a surge, Elisebreen, Svalbard. Quaternary

995   Research 64, 125-137.

996   Croot, D.G., 1988. Glaciotectonics and surging glaciers: a correlation based on

997   Vestspitsbergen, Svalbard, Norway. In: Croot D.G., (Ed.) Glaciotectonics: forms and

998   processes. Balkema, Amsterdam, 49-61.

999   Ćwiąkała, J., Moskalik, M., Forwick, M., Wojtysiak, K., Giżejewski, J., Szczuciński, W., 2018.

1000   Submarine geomorphology at the front of the retreating Hansbreen tidewater glacier,

1001   Hornsund fjord, southwest Spitsbergen. Journal of Maps 14, 123-134.

1002   Dowdeswell, J.A., Drewry, D.J., Liestøl, O., Orheim, O., 1984. Airborne Radio Echo Sounding

1003   of Sub-Polar Glaciers in Spitsbergen. Norsk Polarinstitutt Skrifter 182, 1-41.

1004   Dowdeswell, J.A., Hamilton, G.S., Hagen, J.O., 1991. The duration of the active phase on

1005   surge-type glaciers: contrasts between Svalbard and other regions. Journal of Glaciology

1006   37, 388-400.

1007   Dunér, N., Nordenskiöld, A., 1865. Map of Spitsbergen, Remarks on Geography of

1008   Spitsbergen. Kongl. Svenska Vetenskaps-Akademiens Handlingar 6.

1009   Elverhøi, A., Lønne, Ø., Seland, R., 1983. Glaciomarine sedimentation in a modern fjord

1010   environment, Spitsbergen. Polar Research 1, 127-150.

1011   Etzelmüller, B., Hagen, J.O., 2005. Glacier-permafrost interaction in Arctic and alpine

1012   mountain environments with examples from southern Norway and Svalbard. Geological

1013   Society, London, Special Publications 242, 11-27.

1014 Etzelmüller, B., Hagen, J.O., Vatne, G., Ødegård, R.S., Sollid, J.L., 1996. Glacier debris
1015   accumulation and sediment deformation influenced by permafrost: examples from
1016   Svalbard. Annals of Glaciology 22, 53-62.

1017 Evans, D.J.A, England, J., 1991. High Arctic thrust block moraines. The Canadian
1018   Geographer/Le Géographe canadien 35, 93-97.

1019 Evans, D.J.A., Rea, B.R., 1999. Geomorphology and sedimentology of surging glaciers: a land-
1020   systems approach. Annals of Glaciology 28, 75-82.

1021 Evans, D.J.A., Benn, D.I., 2004. Facies description and the logging of sedimentary exposures.
1022   In: Evans, D.J.A., Benn, D.I., (Eds.), A practical guide to the study of glacial sediments.
1023   Arnold, London, pp. 11-51.

1024 Evans, D.J.A., Rea, B.R., 2005. Late Weichselian deglaciation and sea level history of St
1025   Jonsfjorden, Spitsbergen: A contribution to ice sheet reconstruction. The Scottish
1026   Geographical Magazine 121, 175-201.

1027 Ewertowski, M.W., Evans, D.J.A., Roberts, D.H., Tomczyk, A.M., 2016. Glacial
1028   geomorphology of the terrestrial margins of the tidewater glacier, Nordenskiöldbreen,
1029   Svalbard. Journal of Maps 12, 476-487.

1030 Farnsworth, W.R., Ingólfsson, Ó., Retelle, M., Schomacker, A., 2016. Over 400 previously
1031   undocumented Svalbard surge-type glaciers identified. Geomorphology 264, 52-60.

1032 Farnsworth, W.R., Ingólfsson, Ó., Noormets, R., Allaart, L., Alexanderson, H., Henriksen, M.,
1033   Schomacker, A., 2017. Dynamic Holocene glacial history of St. Jonsfjorden,
1034   Svalbard. Boreas 46, 585-603.

1035 Farnsworth, W.R., Ingólfsson, Ó., Retelle, M., Allaart, L., Håkansson, L.M., Schomacker, A.,
1036   2018. Svalbard glaciers re-advanced during the Pleistocene–Holocene transition. Boreas.

1037 Flink, A.E., Noormets, R. 2018. Submarine glacial landforms and sedimentary environments
1038   in Vaigattbogen, northeastern Spitsbergen. Marine Geology 402, 244-263.

42

1039   Flink, A.E., Noormets, R., Kirchner, N., Benn, D.I., Luckman, A., Lovell, H., 2015. The evolution of a submarine landform record following recent and multiple surges of Tunabreen glacier, Svalbard. Quaternary Science Reviews 108, 37-50.

1042   Flink, A.E., Hill, P., Noormets, R., Kirchner, N., 2017. Holocene glacial evolution of Mohnbukta in eastern Spitsbergen. Boreas.

1044   Forwick, M., Vorren, T.O., Hald, M., Korsun, S., Roh, Y., Vogt, C., Yoo, K.-C., 2010. Spatial and temporal influence of glaciers and rivers on the sedimentary environment in Sassenfjorden and Tempelfjorden, Spitsbergen. In: Howe, J., Austin, W.E.N., Forwick, M., Paetzel, M., (Eds.), Fjord Systems and Archives. Geological Society of London, London.

1049   Glasser, N.F., Hambrey, M.J., Crawford, K.R., Bennett, M.R., Huddart, D., 1998a. The structural glaciology of Kongsvegen, Svalbard, and its role in landform genesis. Journal of Glaciology 44, 136-148.

1052   Glasser, N.F., Huddart, D., Bennett, M.R., 1998b. Ice-marginal characteristics of Fridtjovbreen (Svalbard) during its recent surge. Polar Research 17, 93-100.

1054   Graham, D.J., Midgley, N.G., 2000. Technical Communication - Graphical Representation of Particle Shape using Triangular Diagrams: An Excel Spreadsheet Method. Earth Surface Processes and Landforms 25, 1473-1478.

1057   Gripp, K., 1929. Glaciologische und geologische Ergebnisse der Hamburgischen Spitzbergen-Expedition 1927. Abhandlungen der naturwissenschaftlichen Verein Hamburg, Hamburg.

1060   Hagen, J. O., Liestøl, O., Roland, E., Jørgensen, T., 1993. Glacier atlas of Svalbard and Jan Mayen. Norsk Polarinstitutt Meddelelser 129, 141 pp.

1062   Hald, M., Dahlgren, T., Olsen, T.E., Lebesbye, E., 2001. Late Holocene palaeoceanography in Van Mijenfjorden, Svalbard. Polar Research 20, 23-35.

1064 Hald, M., Ebbesen, H., Forwick, M., Godtliebsen, F., Khomenko, L., Korsun, S., Olsen, L.R.

1065   Vorren, T.O., 2004. Holocene paleoceanography and glacial history of the West

1066   Spitsbergen area, Euro-Arctic margin. Quaternary Science Reviews 23, 2075-2088.

1067 Hamberg, A., 1905. Astronomische, photogrammetrische und erdmagnetische arbeiten der von

1068   AG Nathorst geleiteten Schwedischen Polarexpedition 1898. K Sven. Videnskaps Akad.

1069   Handl, 39.

1070 Hart, J.K., Watts, R.J., 1997. A comparison of the styles of deformation associated with two

1071   recent push moraines, south Van Keulenfjorden, Svalbard. Earth Surface Processes and

1072   Landforms 22, 1089-1107.

1073 Healy, T.R., 1975. Thermokarst—a mechanism of de-icing ice-cored moraines. Boreas 4, 19-

1074   23.

1075 Ingólfsson, Ó., Benediktsson, Í.Ö., Schomacker, A., Kjær, K.H., Brynjólfsson, S., Jonsson, S.

1076   A., Johnson, M.D., 2016. Glacial geological studies of surge-type glaciers in Iceland—

1077   Research status and future challenges. Earth-Science Reviews 152, 37-69.

1078 Kempf, P., Forwick, M., Laberg, J.S., Vorren, T.O., 2013. Late Weichselian and Holocene

1079   sedimentary palaeoenvironment and glacial activity in the high-arctic van Keulenfjorden,

1080   Spitsbergen. The Holocene 23, 1607-1618.

1081 King, E.C., Hindmarsh, R.C.A., Stokes, C.R., 2009. Formation of mega-scale glacial lineations

1082   observed beneath a West Antarctic ice stream. Nature Geoscience 2, 585-588.

1083 King, O., Hambrey, M.J., Irvine-Fynn, T.D., Holt, T.O., 2016. The structural, geometric and

1084   volumetric changes of a polythermal Arctic glacier during a surge cycle:

1085   Comfortlessbreen, Svalbard. Earth Surface Processes and Landforms 41, 162-177.

1086 Kristensen, L., Benn, D.I., 2012. A surge of the glaciers Skobreen–Paulabreen, Svalbard,

1087   observed by time-lapse photographs and remote sensing data. Polar Research 31, 11106.

1088   Kristensen, L., Benn, D.I., Hormes, A., Ottesen, D., 2009a. Mud aprons in front of Svalbard

1089   surge moraines: Evidence of subglacial deforming layers or proglacial glaciotectonics?

1090   Geomorphology 111, 206-221.

1091   Kristensen, L., Juliussen, H., Christiansen, H.H., Humlum, O., 2009b. Structure and

1092   composition of a tidewater glacier push moraine, Svalbard, revealed by DC resistivity

1093   profiling. Boreas 38, 176-186.

1094   Larsen, N.K., Piotrowski, J.A., Christoffersen, P., Menzies, J., 2006. Formation and

1095   deformation of basal till during a glacier surge; Elisebreen,

1096   Svalbard. Geomorphology 81, 217-234.

1097   Larsen, E., Lyså, A., Rubensdotter, L., Farnsworth, W.R., Jensen, M., Nadeau, M.J., Ottesen,

1098   D., 2018. Lateglacial and Holocene glacier activity in the Van Mijenfjorden area, western

1099   Svalbard. arktos 4, 9.

1100   Lawson, D.E., 1982. Mobilization, movement and deposition of active subaerial sediment

1101   flows, Matanuska Glacier, Alaska. The Journal of Geology 90, 279-300.

1102   Liestøl, O., 1969. Glacier surges in west Spitsbergen. Canadian Journal of Earth Sciences 6,

1103   895-897.

1104   Liestøl, O., 1973. Glaciological work in 1971. Norsk Polarinstitutt Årbok 1971, 71–72.

1105   Liestøl, O., 1977. Årsmorener foran Nathorstbreen? Norsk Polarinstitutt Årbok 1976, 361–363.

1106   Liestøl, O., 1988. The glaciers in the Kongsfjorden area, Spitsbergen. Norsk Geografisk

1107   Tidsskrift 42, 231-238.

1108   Lønne, I., 2016. A new concept for glacial geological investigations of surges, based on High-

1109   Arctic examples (Svalbard). Quaternary Science Reviews 132, 74-100.

1110   Lovell, H., Boston, C.M., 2017. Glacitectonic composite ridge systems and surge-type glaciers:

1111   an updated correlation based on Svalbard, Norway. arktos 3.

1112   Lovell, H., Fleming, E.J., Benn, D.I., Hubbard, B., Lukas, S., Rea, B.R., Noormets, R., Flink,
1113   A.E., 2015. Debris entrainment and landform genesis during tidewater glacier surges.
1114   Journal of Geophysical Research: Earth Surface 120, 1574-1595.

1115   Lukas, S., Nicholson, L.I., Ross, F.H., Humlum, O., 2005. Formation, meltout processes and
1116   landscape alteration of High-Arctic ice-cored moraines - examples from Nordenskiöld
1117   Land, central Spitsbergen. Polar Geography 29, 157-187.

1118   Lukas, S., Benn, D.I., Boston, C.M., Brook, M., Coray, S., Evans, D.J., Graf, A., Kellerer-
1119   Pirklbauer, A., Kirkbride, M.P., Krabbendam, M., Lovell, H., Machiedo, M., Mills, S.C.,
1120   Nye, K., Reinardy, B.T., Ross, F.H., Signer, M., 2013. Clast shape analysis and clast
1121   transport paths in glacial environments: A critical review of methods and the role of
1122   lithology. Earth-Science Reviews 121, 96-116.

1123   Lyså, A., Larsen, E.A., Høgaas, F., Jensen, M.A., Klug, M., Rubensdotter, L., Szczuciński, W.
1124   2018. A temporary glacier-surge ice-dammed lake, Braganzavågen, Svalbard. Boreas.

1125   Mangerud, J., Landvik, J.Y., 2007. Younger Dryas cirque glaciers in western Spitsbergen:
1126   smaller than during the Little Ice Age. Boreas 36, 278-285.

1127   Mangerud, J., Svendsen, J.I., 2018. The Holocene Thermal Maximum around Svalbard, Arctic
1128   North Atlantic; molluscs show early and exceptional warmth. The Holocene 28, 65-83.

1129   Mangerud, J., Bondevik, S., Gulliksen, S., Hufthammer, A.K., Høisæter, T., 2006. Marine [14]C
1130   reservoir ages for 19th century whales and molluscs from the North Atlantic. Quaternary
1131   Science Reviews 25, 3228-3245.

1132   Meier, M.F., Post, A., 1969. What are glacier surges? Canadian Journal of Earth Sciences 6,
1133   807-817.

1134   Miller, G.H., Landvik, J.Y., Lehman, S.J., Southon, J.R., 2017. Episodic Neoglacial snowline
1135   descent and glacier expansion on Svalbard reconstructed from the ^{14}C ages of ice-
1136   entombed plants. Quaternary Science Reviews 155, 67-78.

1137 Murray, T., Dowdeswell, J.A., Drewry, D.J., Frearson, I., 1998. Geometric evolution and ice

1138   dynamics during a surge of Bakaninbreen, Svalbard. Journal of Glaciology 44, 263-272.

1139 Murray, T., Strozzi, T., Luckman, A., Jiskoot, H., Christakos, P., 2003. Is there a single surge

1140   mechanism? Contrasts in dynamics between glacier surges in Svalbard and other regions.

1141   Journal of Geophysical Research, 108, 2237.

1142 Nuth, C., Kohler, J., Aas, H.F., Brandt, O., Hagen, J.O., 2007. Glacier geometry and elevation

1143   changes on Svalbard (1936–90): a baseline dataset. Annals of Glaciology 46, 106-116.

1144 Nuth, C., Moholdt, G., Kohler, J., Hagen, J.O., Kääb, A. 2010. Svalbard glacier elevation

1145   changes and contribution to sea level rise. Journal of Geophysical Research: Earth

1146   Surface, 115.

1147 Ó Cofaigh, C., Evans, D.J.A., 2001. Sedimentary evidence for deforming bed conditions

1148   associated with a grounded Irish Sea glacier, southern Ireland. Journal of Quaternary

1149   Science 16, 435-454.

1150 Ottesen, D., Dowdeswell, J.A., 2006. Assemblages of submarine landforms produced by

1151   tidewater glaciers in Svalbard. Journal of Geophysical Research 111.

1152 Ottesen, D., Dowdeswell, J.A., Benn, D.I., Kristensen, L., Christiansen, H.H., Christensen, O.,

1153   Hansen, L., Lebesbye, E., Forwick, M., Vorren, T.O., 2008. Submarine landforms

1154   characteristic of glacier surges in two Spitsbergen fjords. Quaternary Science Reviews

1155   27, 1583-1599.

1156 Ottesen, D., Dowdeswell, J.A., Bellec, V.K., Bjarnadóttir, L.R., 2017. The geomorphic imprint

1157   of glacier surges into open-marine waters: Examples from eastern Svalbard. Marine

1158   Geology.

1159 Philipps, W., Briner, J.P., Gislefoss, L., Linge, H., Koffman, T., Fabel, D., Xu, S., Hormes, A.,

1160   2017. Late Holocene glacier activity at inner Hornsund and Scottbreen, southern

1161   Svalbard. Journal of Quaternary Science 32, 501-515.

1162   Phillips, E., Lee, J.R., Burke, H., 2008. Progressive proglacial to subglacial deformation and

1163   syntectonic sedimentation at the margins of the Mid-Pleistocene British Ice Sheet:

1164   evidence from north Norfolk, UK. Quaternary Science Reviews 27, 1848-1871.

1165   Plassen, L., Vorren, T.O., Forwick, M., 2004. Integrated acoustic and coring investigation of

1166   glacigenic deposits in Spitsbergen fjords. Polar Research 23, 89-110.

1167   Reimer, P.J., Bard, E., Bayliss, A., Beck, J.W., Blackwell, P.G., Bronk Ramsey, C., Grootes,

1168   P.M., Guilderson, T.P., Haflidason, H., Hajdas, I., 2013. IntCal13 and Marine13

1169   radiocarbon age calibration curves 0–50,000 years cal BP. Radiocarbon 55, 1869-1887.

1170   Schellenberger, T., Van Wychen, W., Copland, L., Kääb, A., Gray, L., 2016. An inter-

1171   comparison of techniques for determining velocities of maritime Arctic glaciers,

1172   Svalbard, using Radarsat-2 Wide Fine mode data. Remote Sensing 8, 785.

1173   Sevestre, H., Benn, D.I., 2015. Climatic and geometric controls on the global distribution of

1174   surge-type glaciers: implications for a unifying model of surging. Journal of Glaciology

1175   61, 646-662.

1176   Sevestre, H., Benn, D.I., Luckman, A., Nuth, C., Kohler, J., Lindbäck, K., Pettersson, R., 2018.

1177   Tidewater glacier surges initiated at the terminus. Journal of Geophysical Research: Earth

1178   Surface.

1179   Sharp, M.J., 1985. "Crevasse-fill" ridges—a landform type characteristic of surging glaciers?

1180   Geografiska Annaler: Series A, Physical Geography 67, 213-220.

1181   Sobota, I., Weckwerth, P., Nowak, M., 2016. Surge dynamics of Aavatsmarkbreen, Svalbard,

1182   inferred from the geomorphological record. Boreas 45, 360-376.

1183   Solheim, A., Pfirman, S.L., 1985. Sea-floor morphology outside a grounded, surging glacier;

1184   Bråsvellbreen, Svalbard. Marine Geology 65, 127-143.

1185   Stewart, T.G., 1991. Glacial marine sedimentation from tidewater glaciers in the Canadian

1186   High Arctic. Geological Society of America Special Papers 261, 95-105.

1187 Streuff, K., Forwick, M., Szczuciński, W., Andreassen, K., Ó Cofaigh, C., 2015. Submarine

1188   landform assemblages and sedimentary processes related to glacier surging in

1189   Kongsfjorden, Svalbard. arktos 1.

1190 Streuff, K., Ó Cofaigh, C., Noormets, R., Lloyd, J., 2017a. Submarine landform assemblages

1191   and sedimentary processes in front of Spitsbergen tidewater glaciers. Marine Geology.

1192 Streuff, K., Ó Cofaigh, C., Noormets, R., Lloyd, J.M., 2017b. Submarine landforms and

1193   glacimarine sedimentary processes in Lomfjorden, East Spitsbergen. Marine Geology

1194   390, 51-71.

1195 Sund, M., Eiken, T., 2010. Correspondence: Recent surges on Blomstrandbreen,

1196   Comfortlessbreen and Nathorstbreen, Svalbard, Journal of Glaciology 56, 182-184.

1197 Sund, M., Eiken, T., Hagen, J.O., Kääb, A., 2009. Svalbard surge dynamics derived from

1198   geometric changes. Annals of Glaciology 50, 50-60.

1199 Sund, M., Lauknes, T.R., Eiken, T., 2014. Surge dynamics in the Nathorstbreen glacier system,

1200   Svalbard. The Cryosphere 8, 623-638.

1201 van der Meer, J.J.M., 2004. Spitsbergen Push Moraines. Elsevier, Amsterdam.
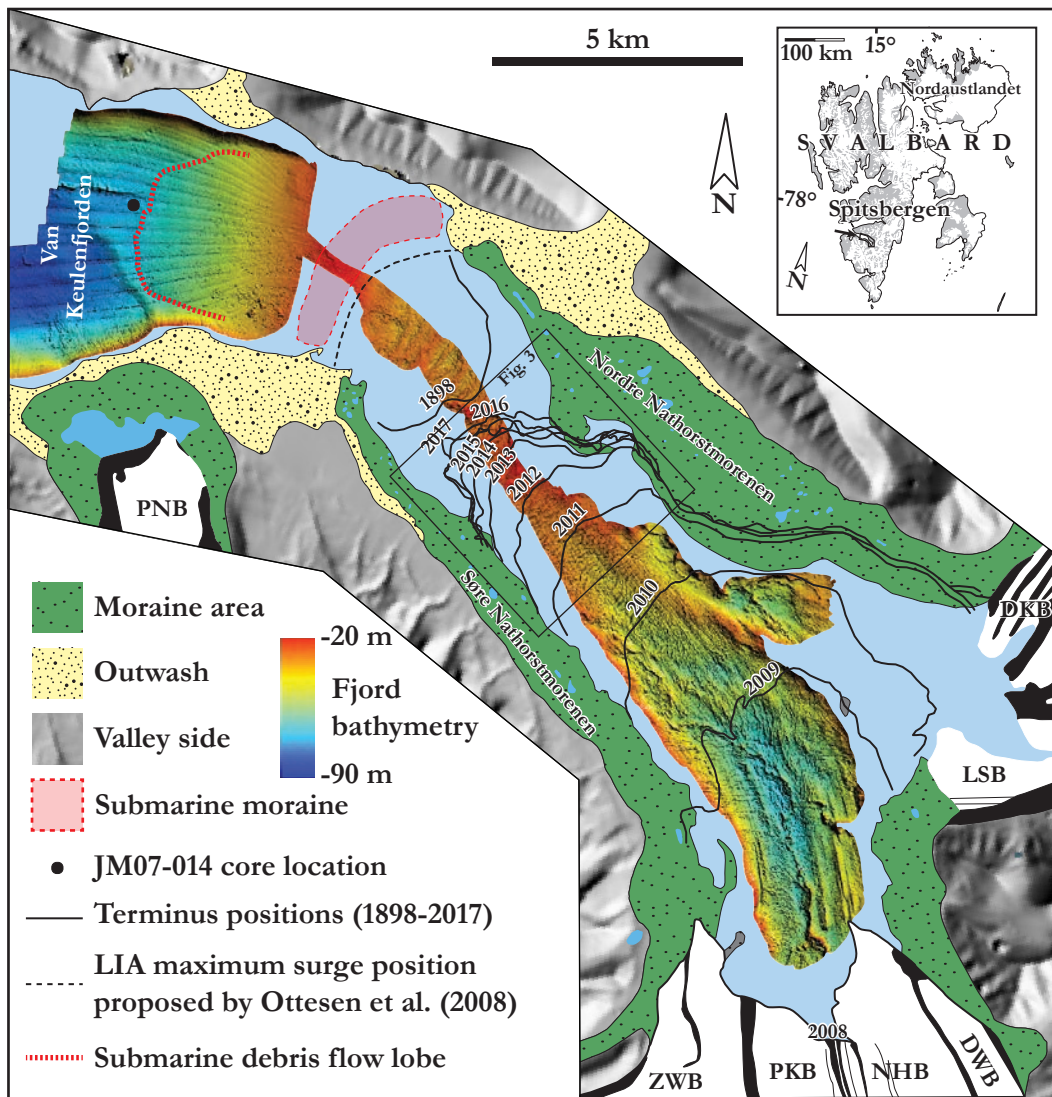
Fig. 1 Map of inner Van Keulenfjorden showing 2008 positions of the flow-units comprising the Nathorstbreen glacier system (NGS) and neighbouring glaciers, and the location of Nordre and Søre Nathorstmorenen. NHB = Nathorstbreen, DKB = Doktorbreen, DWB = Dobrowolskibreen, LSB = Liestølbreen, PKB = Polakkbreen, ZWB = Zawadzkibreen, PNB = Penckbreen. Fjord bathymetry is from Ottesen et al. (2008). Solid black lines show the 2008-2017 frontal positions of NGS and the 1898 positon as mapped by Hamberg (1905). Locations of the submarine moraine and debris flow lobe are based on Ottesen et al. (2008) and Kempf et al. (2013). Core location is from Kempf et al. (2013). Valley side imagery is ArcticDEM data (www.pgc.umn.edu/data/arcticdem). Inset map shows location of Van Keulenfjorden (in black and arrowed) within Svalbard.
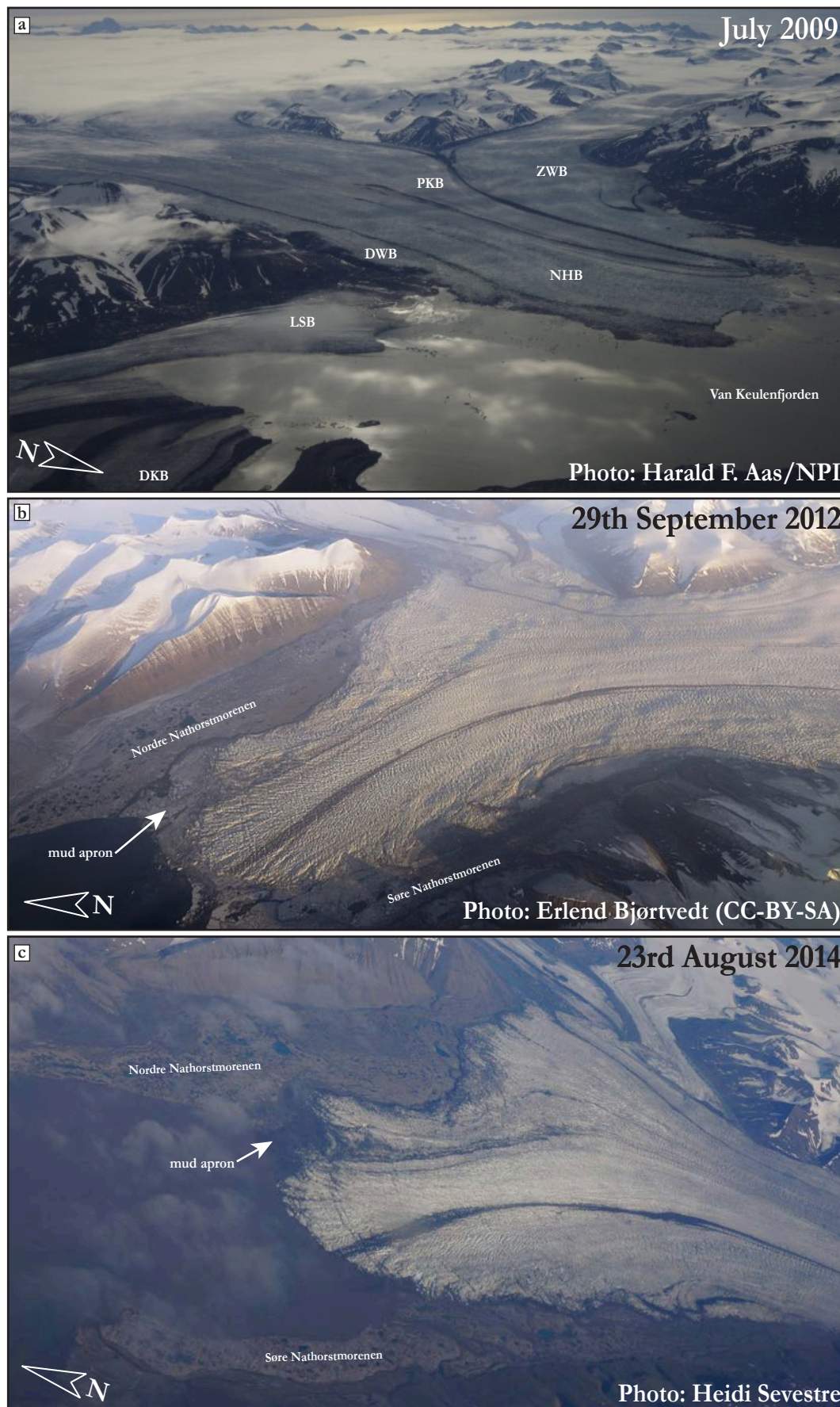
Fig. 2 Aerial photographs of the Nathorstbreen glacier system (NGS) front taken during the frontal advance phase of the recent surge. (a) July 2009, view is to the south-west. The combined front has advanced ~8 km into Van Keulenfjorden since the start of the surge advance phase in 2008. NHB = Nathorstbreen, DKB = Doktorbreen, DWB = Dobrowolskibreen, LSB = Liestølbreen, PKB = Polakkbreen, ZWB = Zawadzkibreen. Photograph acquired from the Norwegian Polar Institute (NPI) TopoSvalbard online archive (toposvalbard.npolar.no). (b) 29th September 2012, view is to the east. NGS has advanced a further ~7 km downfjord since 2009, expanding and filling the bay in front of Liestølbreen and Doktorbreen and spreading laterally onto Nordre and Søre Nathorstmorenen. The proglacial mud apron can be seen at the northern (left-hand) part of the glacier margin where it meets Nordre Nathorstmorenen. (c) 23rd August 2014, view is to the east. The central part of the front has advanced a further ~1 km downfjord since 2012. The proglacial mud apron remains visible at the northern margin.
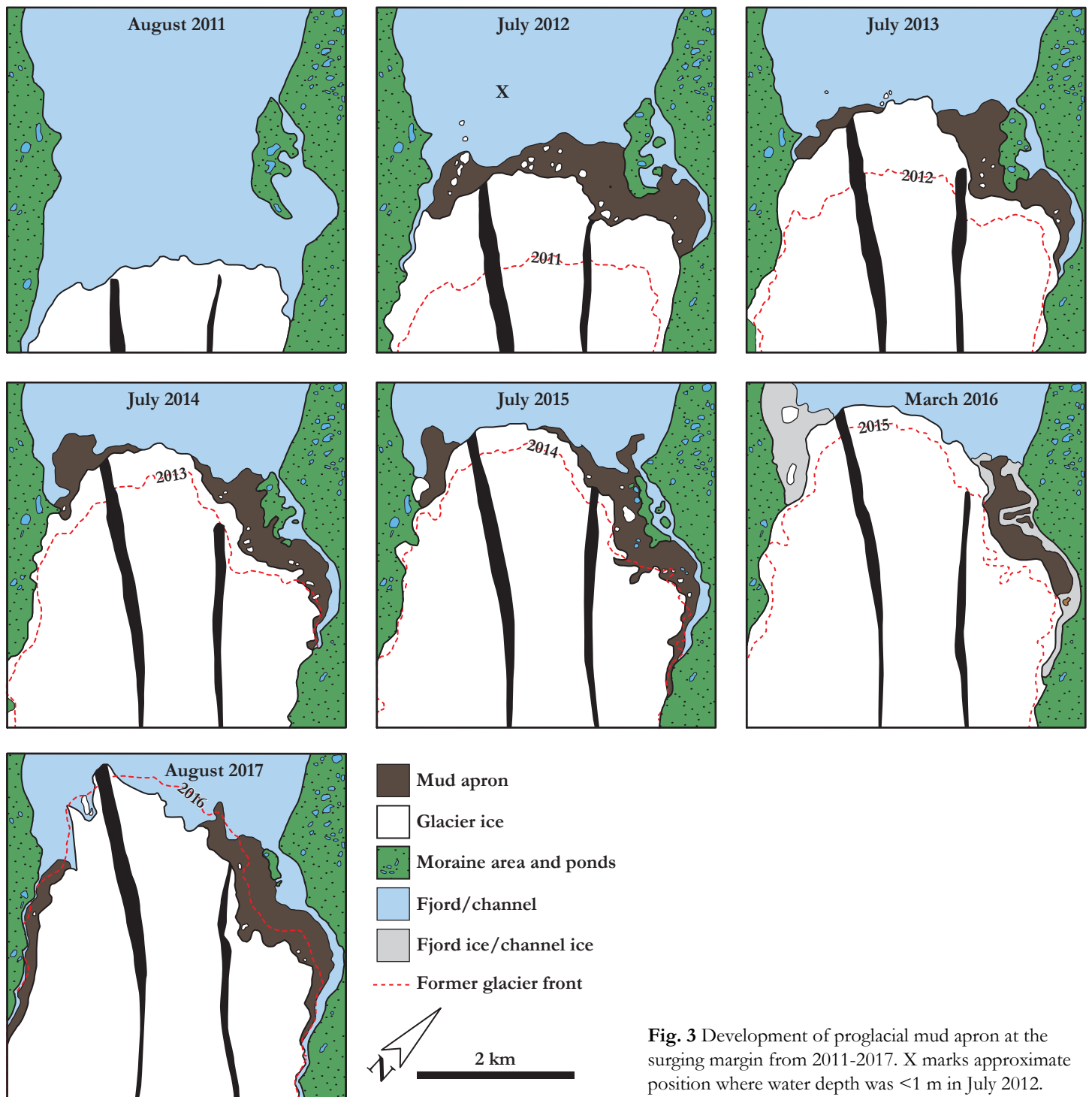
Fig. 3 Development of proglacial mud apron at the surging margin from 2011-2017. X marks approximate position where water depth was <1 m in July 2012.

Legend:
- Mud apron
- Glacier ice
- Moraine area and ponds
- Fjord/channel
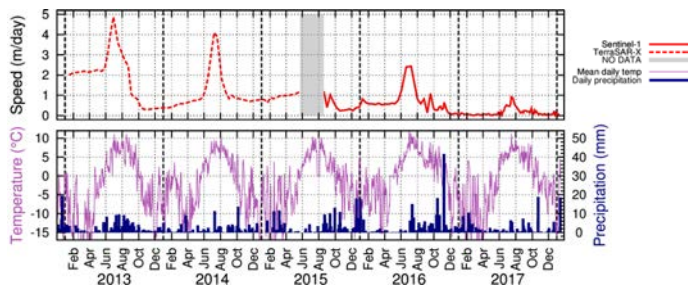- Fjord ice/channel ice
- - - - Former glacier front

2 km

Fig. 4 Surface velocity at the terminus from 2013-2017 derived from feature tracking pairs of TerraSAR-X (dashed line) and Sentinel-1 (solid line) images. Temperature and precipitation data are from the Longyearbyen Airport weather station.

Nordre Nathorstmorenen geometrical ridge orientation

N = 601, 5° classes, 10° interval

Søre Nathorstmorenen geometrical ridge orientation

N = 346, 5° classes, 10° interval

1332±24
1554±51
1419±29
1425±26

NNM02

Nordre Leirodden

NNM01

NNM05 7
NNM03 NNM04 5 6

Van Keulenfjorden

4 2 1
3

NGS

Nordre Nathorstmorenen

Legend

○ Section logs
△ Grain size
🔲 Clast shape } Sample sites
⭐ Shell ¹⁴C ages (uncalibrated)

Fjord
Beach

Channels
Outwash
Ponds
Geometrical ridge
Sinuous ridge

0   2 km

Søre Leirodden

1753±29
1712±25

9710±98
5483±49

9 8

SNM01 SNM02
7406±32

SNM03

Van Keulenfjorden

NGS

Søre Nathorstmorenen

Fig. 5 Geomorphological map of Nordre and Søre Nathorstmorenen showing sediment sections and sample locations. Rose diagr

Fig. 6 The active surging margin of NGS in July 2012. (a) View of the southern margin of the glacier front from Søre Nathorstmorenen. Note large lateral meltwater channel, chaotic crevassing and debris-rich ice. (b) Southern glacier margin and lateral meltwater channel from Søre Nathorstmorenen. Note muddy debris within fracture in the ice (arrowed). (c) Mud apron at northern glacier margin encroaching onto Nordre Nathorstmorenen and geometrical ridges. Note stranded icebergs in the middle ground. Person circled for scale. (d) Mud apron within the fjord at northern glacier margin. View is from Nordre Nathorstmorenen to the south-west. Note small ridges visible on mud apron surface. (e) Large stranded iceberg in Van Keulenfjorden close to southern glacier margin. Note elevated tidal notch at base. (f) Detail of mud apron surface where it has encroached onto Nordre Nathorstmorenen close to northern glacier margin.
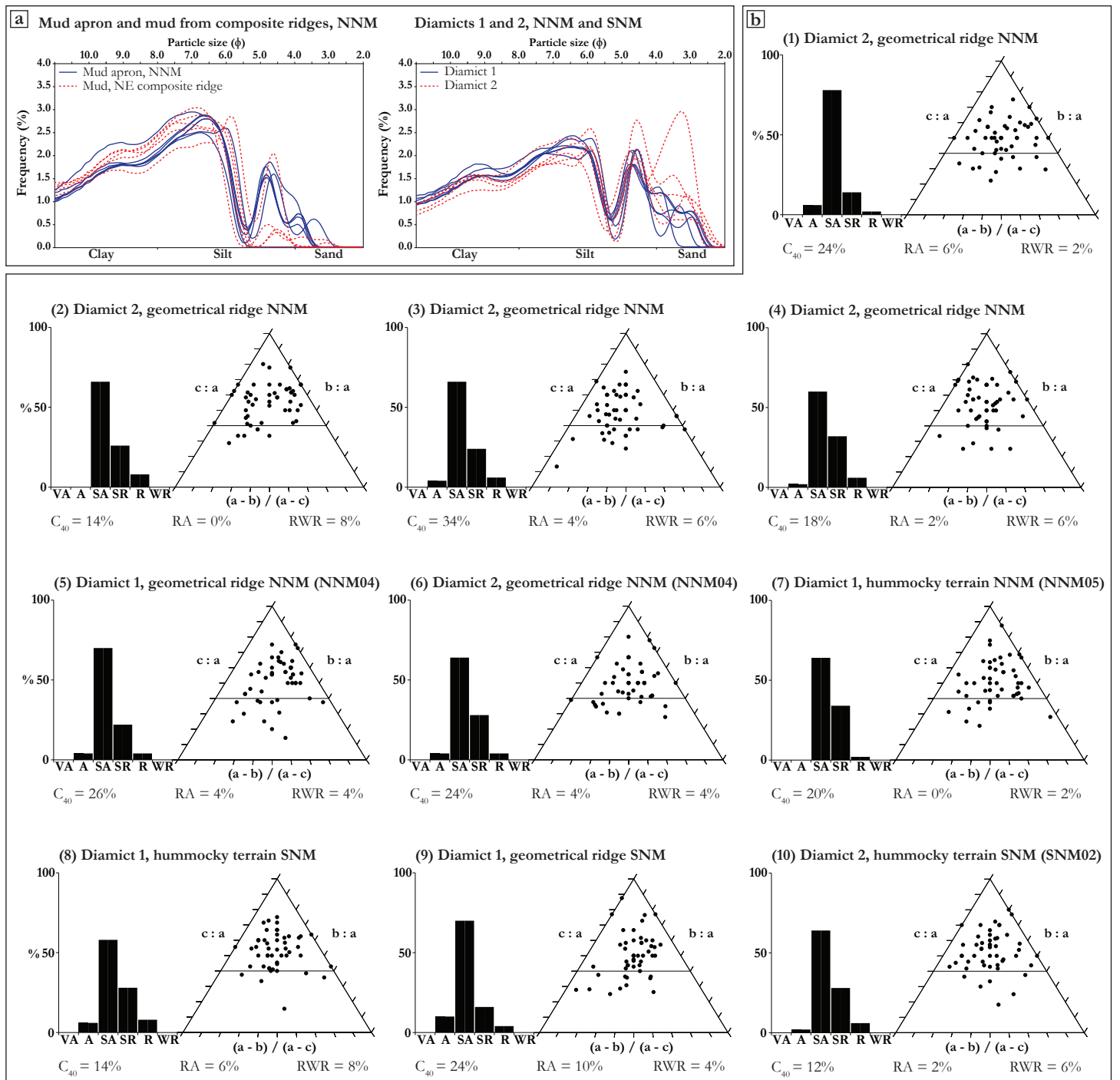
Fig. 7 (a) Grain size distributions of samples taken from the mud apron (n = 6), NE composite ridge system (n = 5), diamict 1 (n = 6) and diamict 2 (n = 5). Sample locations are shown as orange triangles in Fig. 5. (b) Clast shape data plotted on histograms (roundness) and ternary diagrams (shape). Each sample is of 50 sandstone clasts. Numbered sample locations are shown as red squares in Fig. 5. Samples taken from section logs (Figs 12 and 13) have the section log numbers listed in brackets (e.g. NNM04, NNM05).
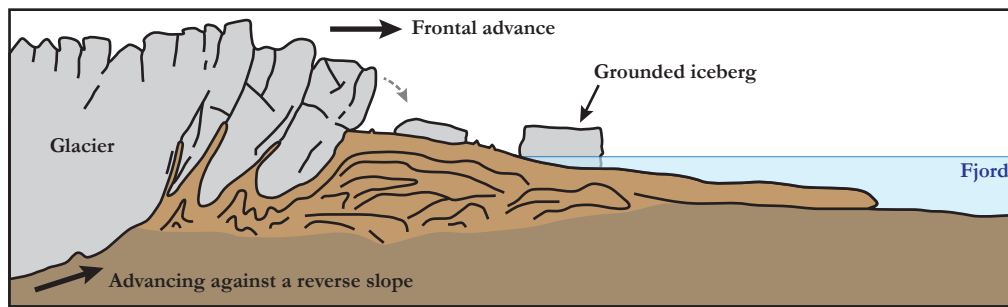
Fig. 8 Formation of proglacial mud apron by glaciotectonic remobilisation of fjord-floor sediments at an advancing margin. Adapted from Kristensen et al. (2009a).
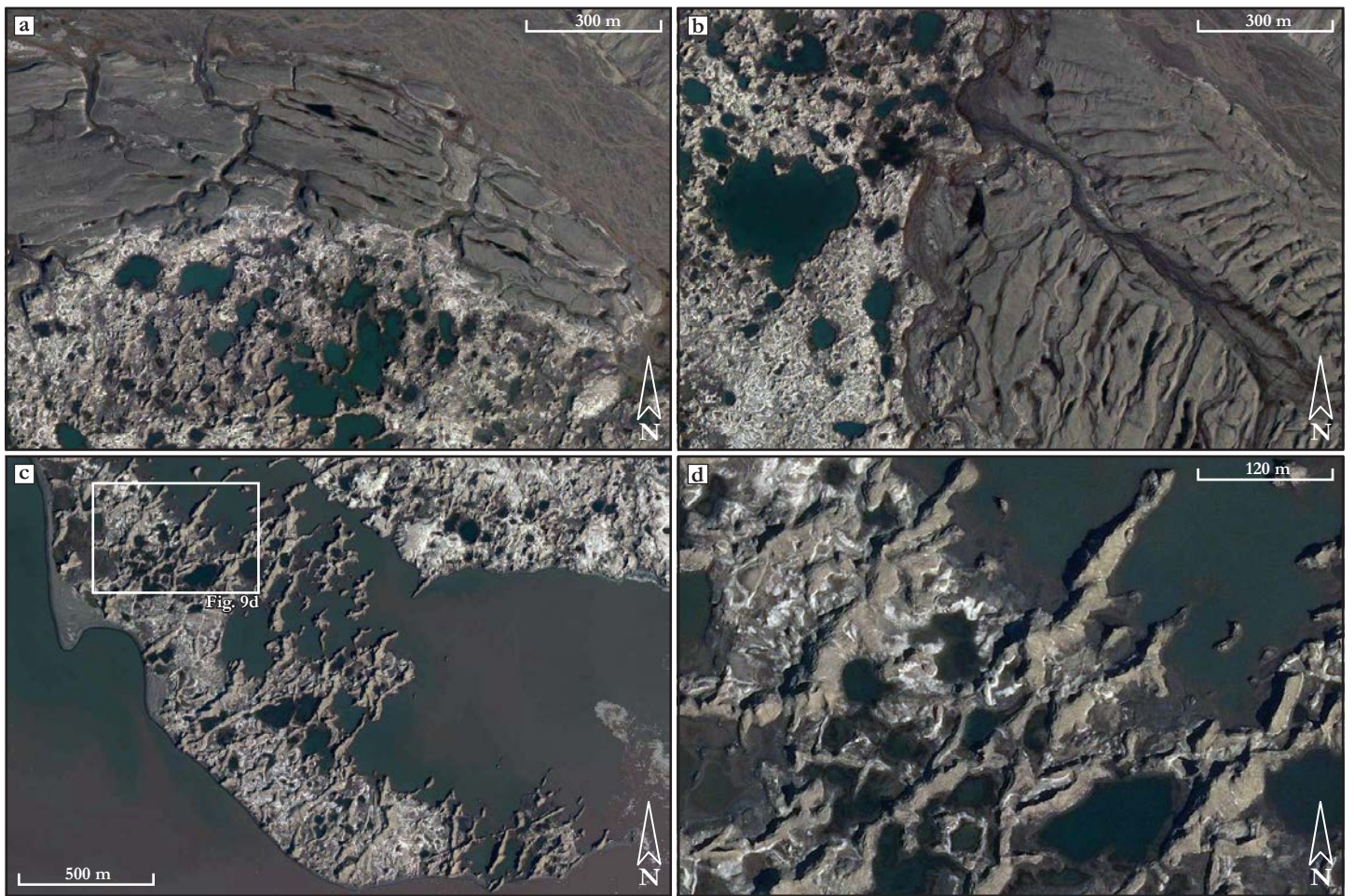
Fig. 9 (a) Boundary between hummocky terrain (bottom) and Nordre Leirodden composite ridge system (top) within Nordre Nathorstmorenen. Note sharp contrast in surface texture and deep channels cut into the composite ridge system. (b) Boundary between hummocky terrain (left) and North-East (NE) composite ridge system (right) within Nordre Nathorstmorenen. Note sharp contrast in surface texture and abundance of meltwater ponds. (c) Geometrical ridges on the spit-like arm of Nordre Nathorstmorenen. (d) Zoomed in view of geometrical ridges in (c). Locations of (a), (b) and (c) are shown on Fig. 5. Aerial photographs are from 2011 and were acquired from the NPI TopoSvalbard online archive.
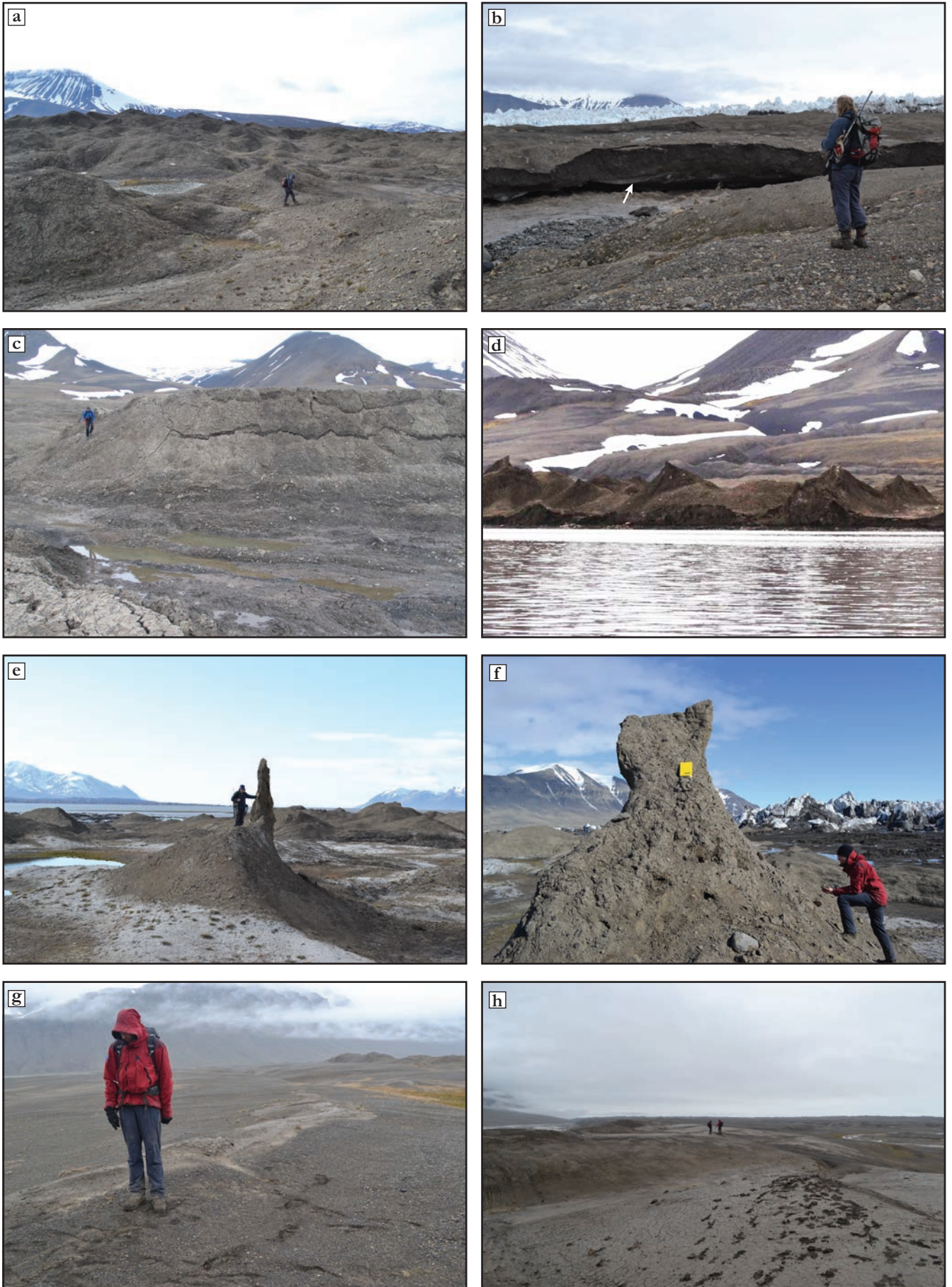
Fig. 10 Examples of terrestrial moraine areas geomorphology. (a) Topography of hummocky terrain and geometrical ridges on Søre Nathorstmorenen. (b) Buried ice (arrowed) in Søre Nathorstmorenen exposed by lateral meltwater channel. (c) Tension cracks in hummocky terrain of Søre Nathorstmorenen. (d) Geometrical ridges on Søre Nathorstmorenen. (e) Free-standing pinnacle on Nordre Nathorstmorenen. (f) Sharp-crested geometrical ridge on the spit-like arm of Nordre Nathorstmorenen. (g) Surface of the Nordre Leirodden composite ridge system. Note the muddy ridge, which represents the surface expression of asymmetric folding. (h) Surface of the North-East (NE) composite ridge system.
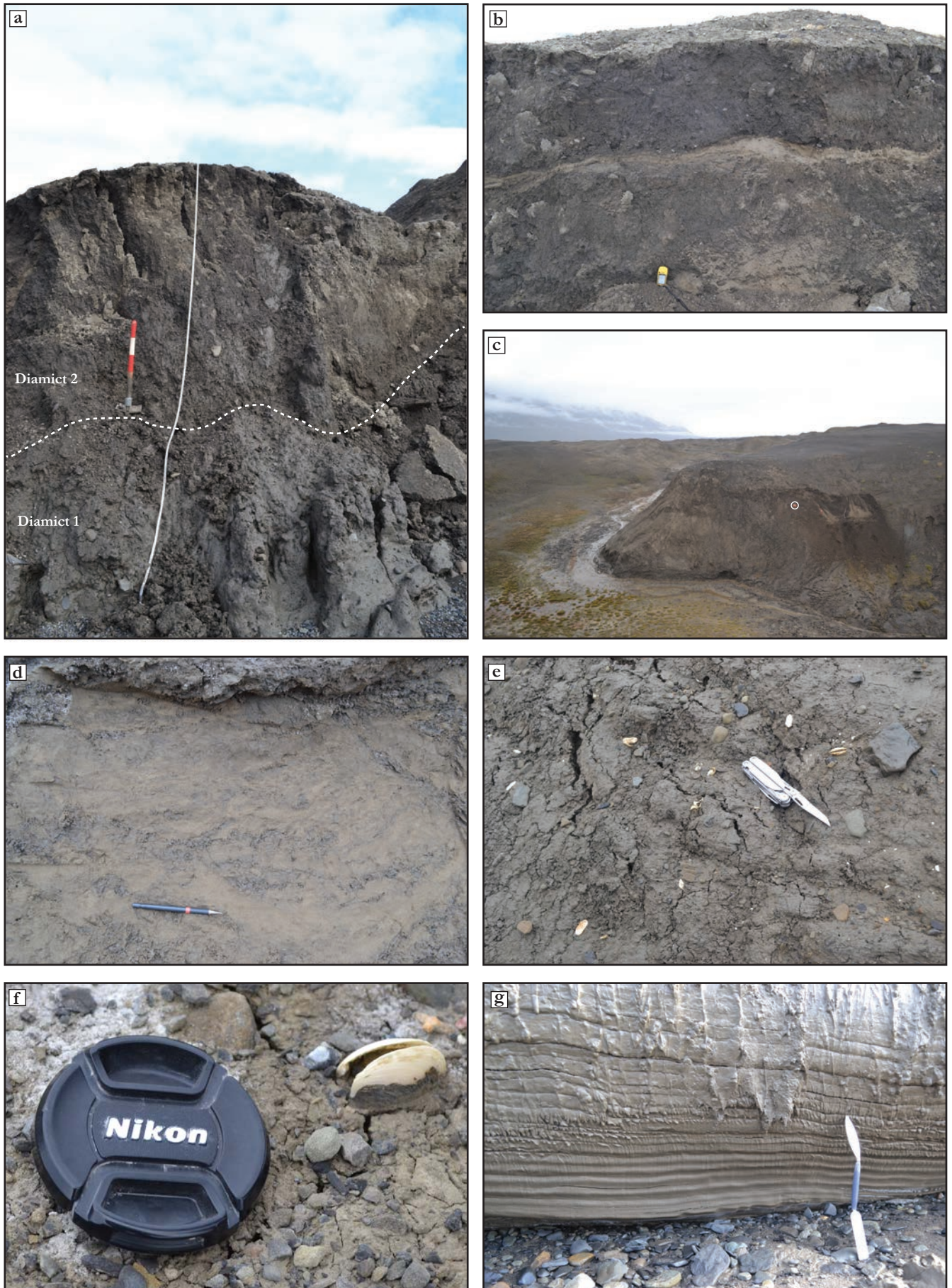
Fig. 11 Examples of terrestrial moraine areas sediment facies. (a) Coastal exposure within geometrical ridge on Nordre Nathorstmorenen showing diamict 1 overlain by diamict 2. See Fig. 12c for section log. (b) Sand layers within diamict 2, Søre Nathorstmorenen. (c) Internal structure of part of the Nordre Leirodden composite ridge system. Flare gun circled for scale. See Fig. 12e for section log. (d) Sheared sand and clay lenses in Søre Nathorstmorenen coastal exposure. See Fig. 13a for section log. (e) Hiatella arctica paired shells sampled from the surface of the NE composite ridge system for radiocarbon dating. (f) Paired bivalve shells sampled from diamict 1 on the surface of the Søre Nathorstmorenen for radiocarbon dating. (g) Wavy-laminated clay/silt couplets in coastal exposure within Nordre Nathorstmorenen. See Fig. 12b for section log.
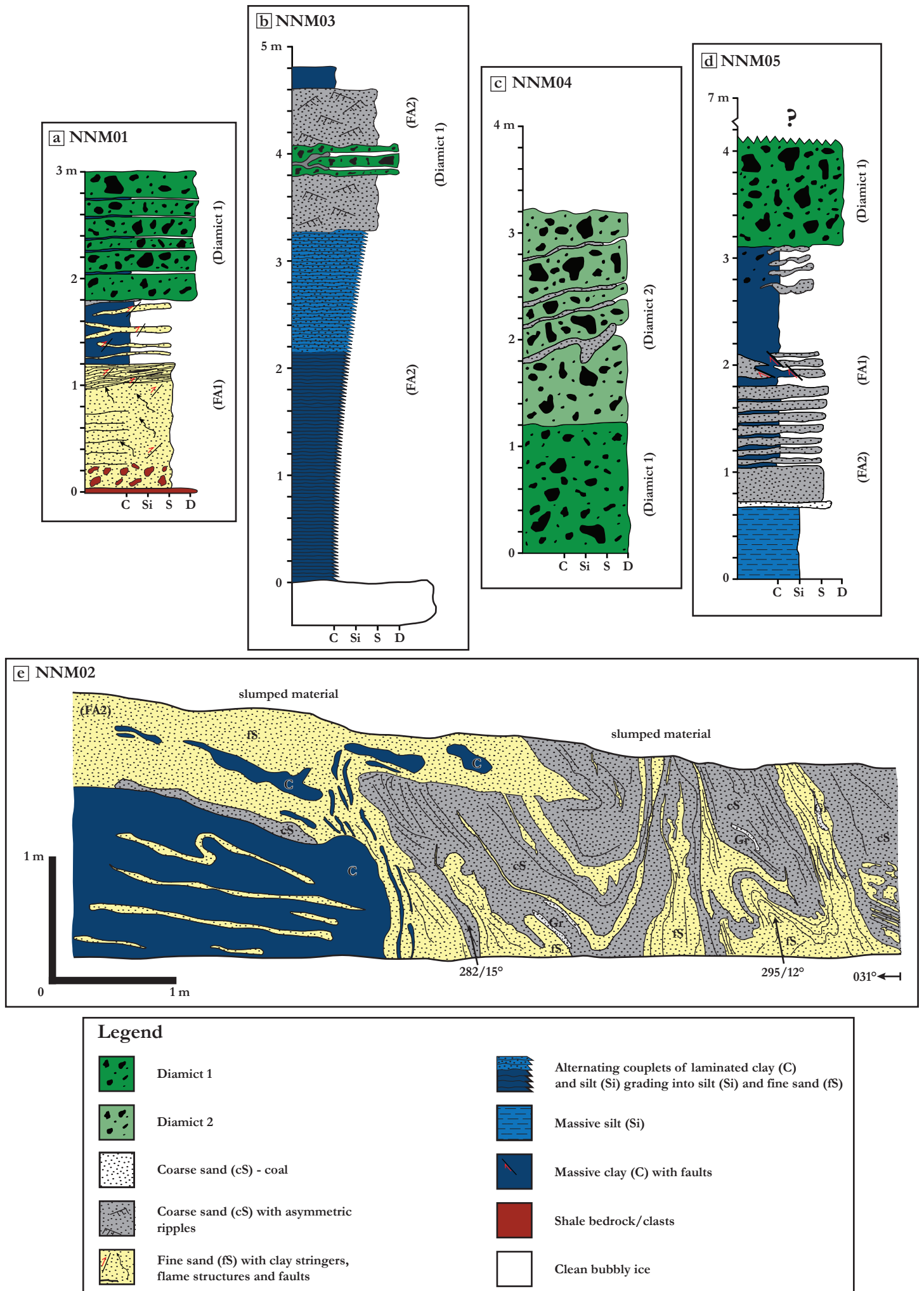
Fig. 12 Nordre Nathorstmorenen section logs. (a) NNM01. (b) NNM03. (c) NNM04. (d) NNM05. (e) NNM02. See Fig. 5 for locations.
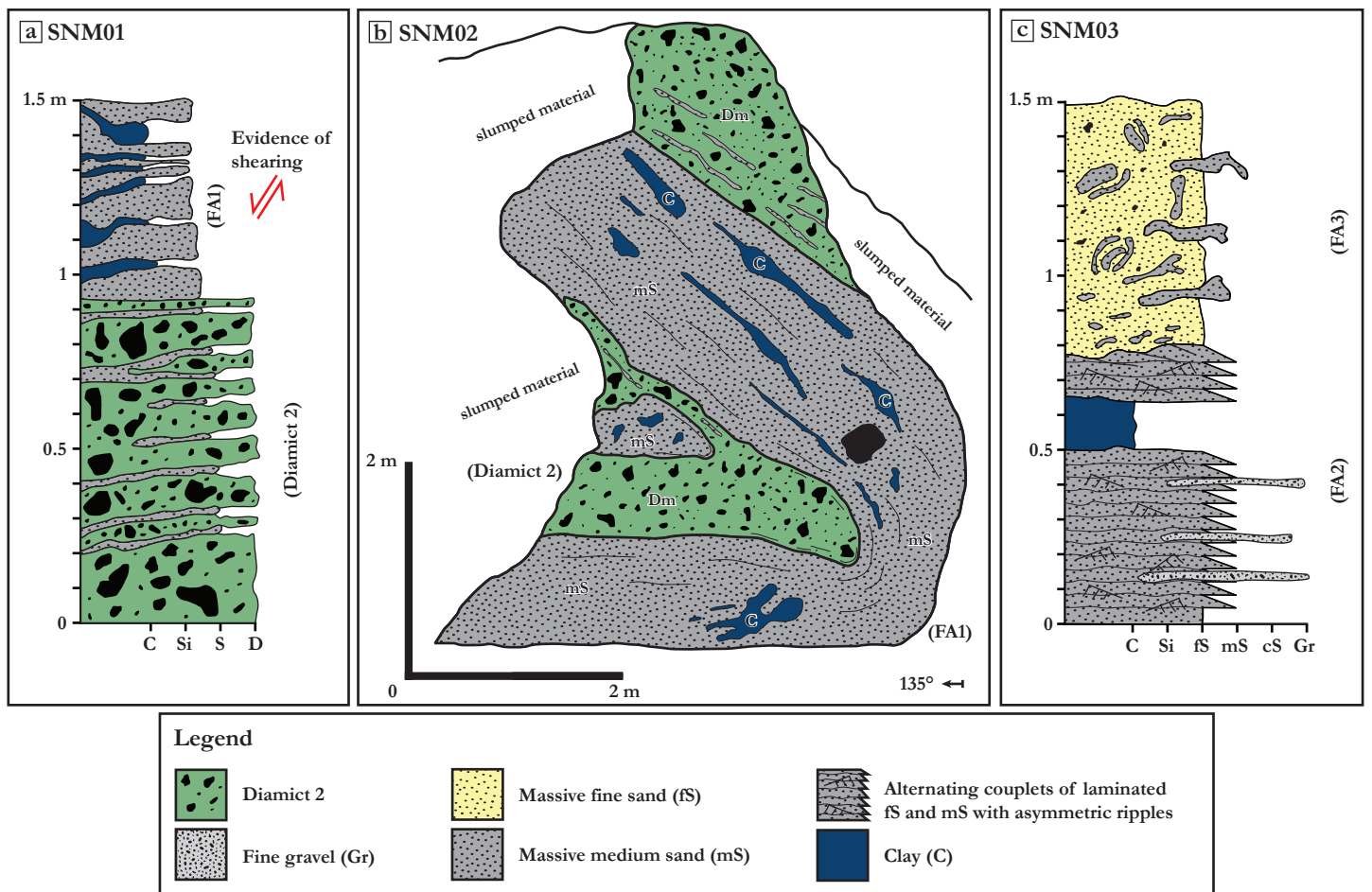
Fig. 13 Søre Nathorstmorenen section logs. (a) SNM01. (b) SNM02. (c) SNM03. See Fig. 5 for locations.
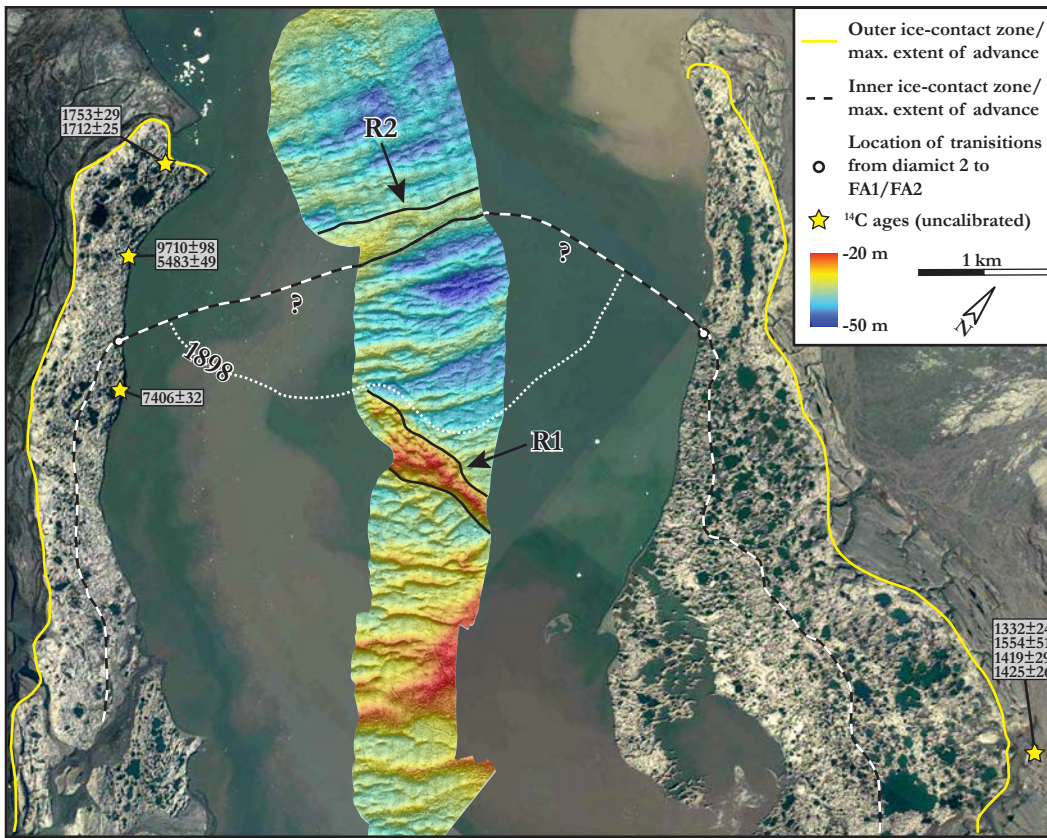
Fig. 14 Correlation of terrestrial and submarine evidence for two ice-contact zones within inner Van Keulenfjorden. Locations and uncalibrated radiocarbon ages of sampled shells are shown (see Table 1). 1898 margin position (white dotted line) is from Hamberg (1905). Fjord bathymetry is from Ottesen et al. (2008). Aerial photograph is from the NPI TopoSvalbard online archive.
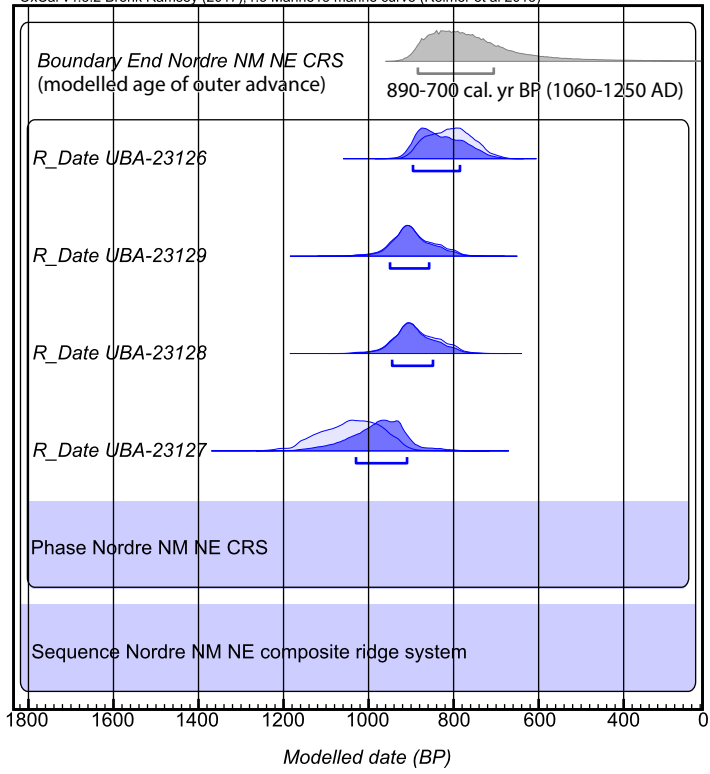
Fig. 15 Modelled age ranges for the four Hiatella arctica radiocarbon dates from the NE composite ridge system and shown in dark blue. Calibrated ages are presented within a phase model (Bronk Ramsey and Lee, 2013). The age estimate of the outer advance is shown in grey. All ages have been calibrated with the Marine13 radiocarbon calibration curve (Reimer et al., 2013) and an additional marine reservoir correction (ΔR) of 70±30 years (after Mangerud et al., 2006; Mangerud and Svendsen, 2018). Ages are given in years BP with a 1σ confidence limit. See Appendix 1 for the OxCal code used in the model.
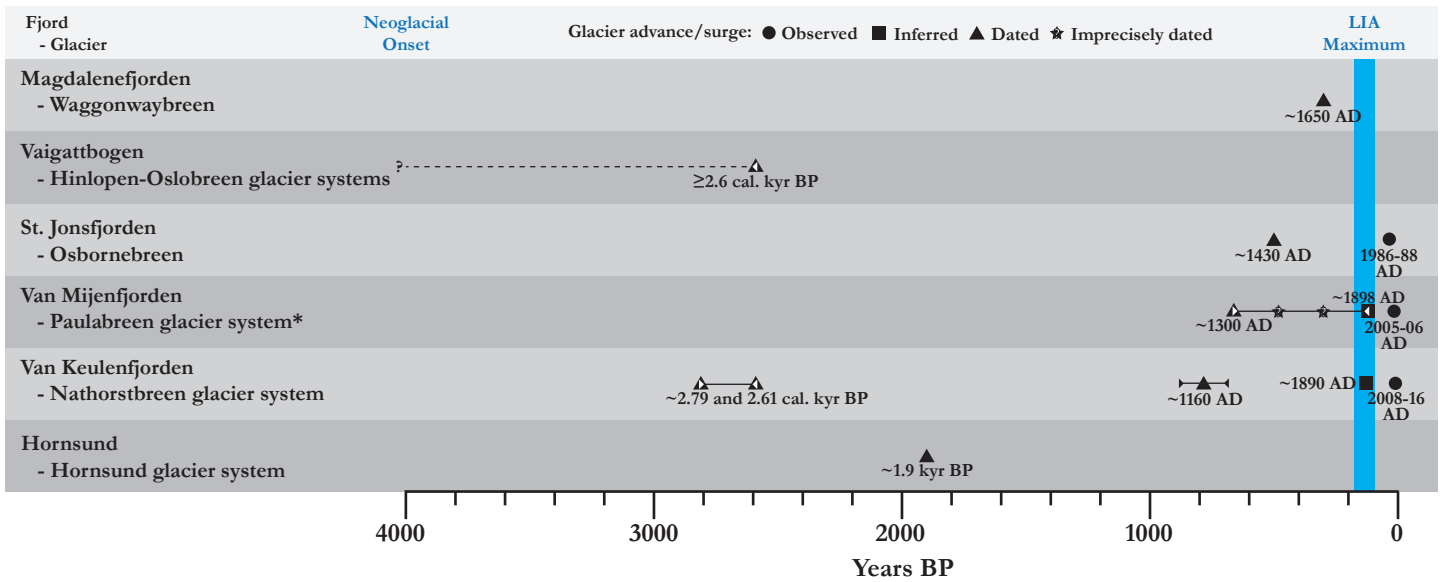
Fig. 16 Svalbard tidewater glacier systems with dated pre-Little Ice Age advances since the onset of the Neoglacial period, some of which have been interpreted as glacier surges. Ages younger than 1000 yr BP are presented as years AD. Data sources for further details on these glaciers and the presented advance ages are as follows: Waggonwaybreen (Streuff et al., 2017a), Hinlopen-Oslobreen glacier systems (Flink and Noormets, 2018), Osbornebreen (Dowdeswell et al., 1991; Evans and Rea, 2005; Farnsworth et al., 2017), Paulabreen (Hald et al., 2001; Ottesen et al., 2008; Kristensen et al., 2009a; Larsen et al., 2018; Lyså et al., 2018), Nathorstbreen glacier system (Ottesen et al., 2008; Kempf et al., 2013; this study), Hornsund glacier system (Philipps et al., 2017). The imprecisely dated surges of Paulabreen are based on Larsen et al. (2018), who identified two additional surges from the submarine geomorphological record that occurred sometime between the dated ~1300 AD surge and the inferred surge in ~1898 . These are shown equally spaced between these dates (with a wide error bar) for illustration purposes only.

Table 1. Uncalibrated and calibrated radiocarbon ages of bivalve shells. See Fig. 5 for locations of sampled shells. Calibration was carried out using the Marine13 curve (Reimer et al., 2013) and a marine reservoir correction with a ΔR value of 70±30 (Mangerud et al., 2006; Mangerud and Svendsen, 2018). *Radiocarbon ages from the same single pair of bivalve shells.

Sample ID	Location (UTM – 33X)	Moraine and sediment facies	Dated material	Lab code	Age (^{14}C yr BP)	Age (cal. yr BP; 1σ)
NNM1	E 527370, N 8605300	Nordre NM NE composite ridge system, FA1 massive clay (surface)	*H. arctica* (paired)	UBA-23126	1332±24	750-870
NNM2	E 527370, N 8605300	Nordre NM NE composite ridge system, FA1 massive clay (surface)	*H. arctica* (paired)	UBA-23127	1554±51	950-1110
NNM3	E 527370, N 8605300	Nordre NM NE composite ridge system, FA1 massive clay (surface)	*H. arctica* (paired)	UBA-23128	1419±29	830-950
NNM4	E 527370, N 8605300	Nordre NM NE composite ridge system, FA1 massive clay (surface)	*H. arctica* (paired)	UBA-23129	1425±26	850-960
SNM1	E 520520, N 8603480	Søre NM, diamict 2 (section)	*H. arctica* (single)	UBA-23883	7406±32	7730-7860
SNM2	E 519900, N 8604250	Søre NM, diamict 1 (section)	*H. arctica* (single)	UBA-30080	9710±98	10380-10660
SNM3	E 519900, N 8604250	Søre NM, diamict 1 (section)	*H. arctica* (single)	UBA-30079	5483±49	5720-5870
SNM4	E 519580, N 8605070	Søre NM diamict 1 (surface)	*Unidentified* (single shell of pair)*	UBA-29381	1753±29	1200-1290
SNM5	E 519580, N 8605070	Søre NM diamict 1 (surface)	*Unidentified* (single shell of pair)*	UBA-29382	1712±25	1170-1260

Appendix 1. OxCal code for age model used for Fig. 15.

```
Plot()
{
 Curve("Marine13","Marine13.14c");
 Delta_R("Local",N(70, 30));
 Sequence("Nordre NM NE composite ridge system")
 {
 Boundary("Start Nordre NM NE CRS")
  {
   color="grey";
  };
 Phase("Nordre NM NE CRS")
  {
  R_Date("UBA-23127", 1554, 51)
   {
    color="blue";
   };
  R_Date("UBA-23128", 1419, 29)
   {
    color="blue";
   };
  R_Date("UBA-23129", 1425, 26)
   {
    color="blue";
   };
  R_Date("UBA-23126", 1332, 24)
   {
    color="blue";
   };
  Span("Span of dates (Nordre NM NE CRS Phase)")
   {
    color="grey";
   };
  };
 Boundary("End Nordre NM NE CRS")
  {
  color="grey";
  };
 };
};
```